



1 Channel cross-section heterogeneity of particulate organic carbon 2 transport in the Huanghe

3 Yutian Ke^{1†}, Damien Calmels¹, Julien Bouchez², Marc Massault¹, Benjamin Chetelat³, Aurélie
4 Noret¹, Hongming Cai², Jiubin Chen³, Jérôme Gaillardet², Cécile Quantin¹

5 ¹GEOPS, Université Paris-Saclay-CNRS, 91405 Orsay, France

6 ²Université de Paris, Institut de Physique du Globe de Paris, CNRS, 75005 Paris, France

7 ³School of Earth System Science, Institute of Surface-Earth System Science, Tianjin University, 300072 Tianjin,
8 China

9 [†]Present address: Division of Geological and Planetary Science, California Institute of Technology, Pasadena, CA
10 91125, USA

11 *Corresponding author:* Yutian KE (yutianke@caltech.edu)

12 **Abstract.** The Huanghe (Yellow River), one of the largest turbid river systems in the world, has long been recognized
13 as a major contributor of suspended particulate matter (SPM) to the ocean. However, over the last few decades, the
14 SPM export flux of the Huanghe has decreased over 90% due to the high management, impacting the global export of
15 particulate organic carbon (POC). To better constrain sources and modes of transport of POC beyond the previously
16 investigated transportation of POC near the channel surface, SPM samples were for the first time collected over a
17 whole channel cross-section in the lower Huanghe. Riverine SPM samples were analyzed for particle size and major
18 element contents, as well as for POC content and dual carbon isotopes (¹³C and ¹⁴C). The results show clear vertical
19 and lateral heterogeneity of SPM physical and chemical characteristics within the river cross-section, with for example
20 finer SPM carrying more POC with higher ¹⁴C activity near the surface of the right bank. Notably, we discuss how
21 bank erosion in the alluvial plain is likely to generate lateral heterogeneity in POC composition. The Huanghe POC
22 is millennial-aged (4,020 ± 500 radiocarbon years), dominated by organic carbon (OC) from the biosphere, while the
23 lithospheric fraction reaches up to ca. 33%. The mobilization of aged and refractory OC, including radiocarbon-dead
24 biospheric OC, from deeper soil horizons of the loess-paleosol sequence through erosion in the Chinese Loess Plateau
25 is an important mechanism contributing to fluvial POC in the Huanghe drainage basin. Altogether, anthropogenic
26 activities can drastically change the compositions and transport dynamics of fluvial POC, consequentially altering the
27 feedback of the source-to-sink trajectory of a river system to regional and global carbon cycles.



28 **1 Introduction**

29 Rivers are the main conveyor of rock and soil debris eroded from the continents to the ocean. Along with inorganic
30 material, river sediments host particulate organic carbon (POC) derived mainly from three major sources: 1) recently
31 photosynthesized OC of the biosphere, 2) aged and altered OC from soils, and 3) ancient OC contained in sedimentary
32 rocks (Blair et al., 2010). The net effect of riverine POC transport on the carbon cycle and thus on the evolution of
33 Earth's climate depends on POC provenance and fate. The effective sedimentary burial of POC derived from the
34 terrestrial biosphere (biospheric OC, OC_{bio}) represents a net, long-term sink of atmospheric CO_2 (Galy et al., 2007,
35 Bouchez et al., 2014; Hilton et al., 2015), whereas the oxidation of POC derived from continental rocks (petrogenic
36 OC, OC_{petro}) acts as a net, long-term source of CO_2 to the atmosphere (Hilton et al., 2014). The erosion and burial of
37 OC_{petro} escaping from oxidation has no net effect on the long-term carbon cycle (Galy et al., 2008a; Bouchez et al.,
38 2010; Hilton et al., 2011; Horan et al., 2019). In addition, the reactive nature of OC_{bio} might also result in short-term
39 CO_2 emission during transport from both river channels and recently-deposited sediments (Mayorga et al., 2005; Galy
40 and Eglinton, 2011; Blair and Aller, 2012).

41 Globally, rivers transport a total POC flux of *ca.* 200 Tg C/year, consisting of 157^{+74}_{-50} Tg C/year of OC_{bio} and 43^{+61}_{-25}
42 Tg C/year of OC_{petro} (Galy et al., 2015; Ludwig et al., 1996). Source-to-sink processes controlling the origin and fate
43 of riverine POC are prominently river-specific, suggesting that the impact of POC on regional and global carbon
44 cycles might significantly vary both spatially and temporally (Blair and Aller, 2012). It is thus crucial to understand
45 the mechanisms controlling the POC export by large rivers that integrate vast portions of the land surface, and quantify
46 the differing sources of carbon exported by those large river systems.

47 The Huanghe (Yellow River) is a highly turbid river system that exports over 85% of its OC as particulate matter,
48 with efficient deposition and preservation in the ocean (Cauwet and Mackenzie, 1993; Bianchi, 2011; Zhang et al.,
49 2013; Ran et al., 2013). The Huanghe has been highly managed over the last few decades through water and soil
50 conservation measures as well as reservoir construction, leading to a decrease of nearly 90% of its sediment load
51 (Wang and Fu et al., 2016; Wang et al., 2007; Milliman et al., 1987) and a significant decrease in its POC delivery to
52 the ocean (Zhang et al., 2013). Reservoir construction dramatically affects the transport and fate of both sediment load
53 and POC in large rivers (Syvitski et al., 2005; Li et al., 2015). The estimated POC flux of the Huanghe is thought to
54 have shifted from 4.5 Tg C/yr in the 1980s (Cauwet and Mackenzie, 1993) to 0.34-0.58 Tg C/yr nowadays (Tao et al.,
55 2018) in response to both anthropogenic influence (Hu et al., 2015; Tao et al., 2018; Yu et al., 2019a) and natural
56 variability of the regional hydrological cycle (Qu et al., 2020). These large-scale perturbations have likely modified
57 the OC input from the different terrestrial pools as well as the fate of exported POC that was previously reaching
58 deposition centers in the ocean and that now remains stuck on land. Those alterations of the carbon cycle remain to
59 be addressed.

60 Over the last decade, POC transport in the Huanghe has been investigated for 1) determination and quantification of
61 POC sources, based on bulk or molecular carbon isotopic composition (Tao et al., 2015; Yu et al., 2019b; Ge et al.,
62 2020; Qu et al., 2020); 2) temporal and spatial variations in POC export and distribution among different size fractions
63 (Ran et al., 2013; Wang 2012; 2016; Yu et al., 2019a, b, Qu et al., 2020); 3) impact of anthropogenic activities (Hu et



64 al., 2015; Tao et al., 2018; Yu et al., 2019a); and 4) burial efficiency and preservation in the ocean (Sun et al., 2018;
65 Tao et al., 2016; Ge et al., 2020). However, all these previous studies rely on suspended sediment samples collected
66 near the channel surface or at a single, intermediate depth in the river channel, further assuming a homogeneous
67 distribution of suspended sediment characteristics in the water column, both vertically and laterally. It is now well
68 recognized that suspended sediments present physical, mineralogical, chemical, and isotopic heterogeneities across
69 river cross-sections due to hydrodynamic sorting and tributary mixing (Galy et al., 2008b; Garzanti et al., 2010;
70 Bouchez et al., 2010, 2011a). This is also true for POC, whose age and composition vary within cross-sections (*e.g.*,
71 Bouchez et al., 2014; Baronas et al., 2020) and between sediment size fractions separated in the laboratory (Yu et al.,
72 2019b; Ge et al., 2020). Such heterogeneity warrants a re-evaluation of POC transport in the Huanghe, accounting for
73 the variability in suspended sediment characteristics over the channel cross-section.

74 In this study, we take advantage of in-river hydrodynamic sorting to access the full range of suspended sediment size
75 fractions by collecting suspended particulate matter (SPM) samples along several river depth profiles distributed
76 across a channel transect (*e.g.*, Bouchez et al., 2014; Freymond et al., 2018; Baronas et al., 2020). We apply this
77 sampling scheme to a cross-section of the Huanghe located 200 km upstream from the river mouth and report SPM
78 OC content, stable isotope composition, and radiocarbon activity as well as total nitrogen, major element composition
79 (aluminum and silicon), and particle size distribution. Based on these novel samples and data sets, this study aims at
80 1) determining the controls on POC content in the Huanghe; 2) tracing and quantifying the sources of riverine POC
81 in the Huanghe; and 3) providing depth-integrated estimates of POC fluxes in the most turbid large river system.

82 **2 Study area**

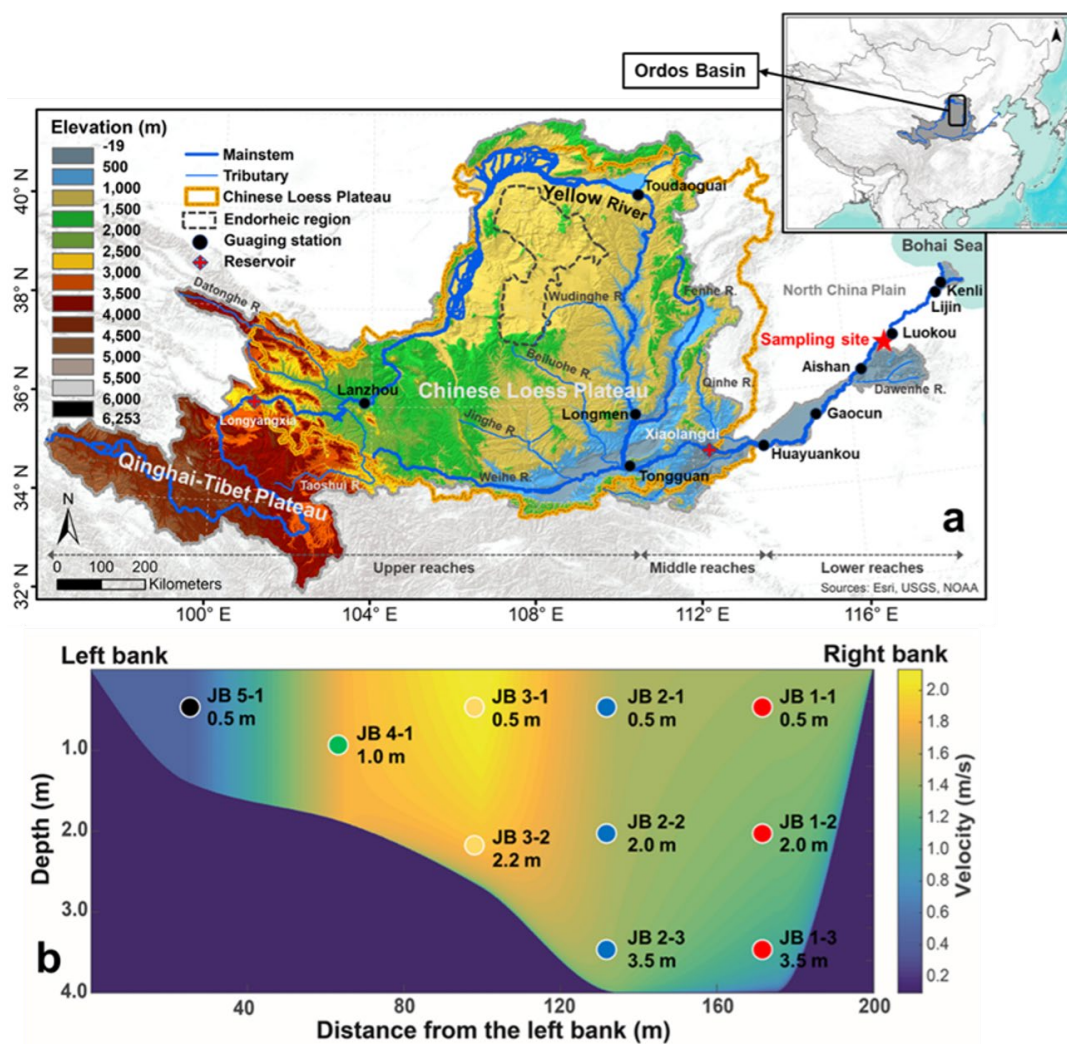
83 The Huanghe originates from the north-eastern Qinghai-Tibet Plateau (QTP) and runs through the Chinese Loess
84 Plateau (CLP) and the North China Plain (NCP) to the Bohai Sea (Figure 1a). It is 5,464 km long and drains a basin
85 area of 79.5×10^4 km². The Huanghe drainage basin can be subdivided into three main geomorphic units: 1) the high-
86 relief upper reaches spanning from the source region (elevation of 4,500 m) to the city of Toudaoguai (located 3,472
87 km downstream at an elevation of 1,000 m); 2) the middle reaches with a channel length of 1,206 km, ending at
88 Huayankou (elevation of 110 m) draining landscapes characterized by relatively gentle slopes; and 3) the lower
89 reaches where the river flows eastwards across a fluvial plain over a length of 786 km. These three sections drain
90 53.8%, 43.3%, and 2.9% of the whole Huanghe basin area, respectively (Wang et al., 2007; YRCC, 2016). Most
91 second-order tributaries drain the CLP region and feed the main channel in the middle reaches, the Dawenhe River
92 being the only tributary of the lower reaches, with negligible water and sediment supply due to upstream trapping in
93 lakes and reservoirs. It is worth noting that more than 50% of the water discharge at the Huanghe's mouth comes from
94 the QTP, whereas over 90% of the sediment load originates from the CLP (Wang et al., 2010, 2017; Pan et al., 2016).
95 The CLP is thus the principal source area of sediment to the Huanghe (Shi and Shao, 2000; Guo et al., 2002; Wang
96 and Fu et al., 2016).

97 The Huanghe drainage basin is mostly underlain by the North China craton, and is bounded by several mountain belts.
98 The watershed encompasses 46% of sedimentary rock outcrops (mainly siliciclastic rocks with minor carbonates), and
99 about 45% of unconsolidated sediments (mainly Quaternary loess deposits). The remaining outcrops include



100 metamorphic, plutonic, and volcanic rocks formed from the Archean to the Tertiary (Figure S1). Although river
101 incision is strong in the QTP, a substantial part of the corresponding eroded material is not effectively transferred to
102 the lower reaches due to deposition in the CLP and the western Mu-Us desert, a situation that has prevailed since at
103 least the middle Pleistocene (Nie et al., 2015; Licht et al., 2016; Pan et al., 2016). In addition, recent anthropogenic
104 disturbance such as constructions of large dams in the upper reaches has profoundly modified the export of solid
105 materials from the basin (Wang et al., 2007). The Huanghe then flows through the CLP that has acted as the major
106 supplier of sediment to the system since at least the Calabrian Pleistocene (Stevens et al., 2013; Bird et al., 2015).
107 There, an easily erodible loess-paleosol formation has accumulated since 2.58 Ma (Guo et al., 2002), over a thickness
108 ranging from a few meters to more than 500 m, with an average of 100 m. This loess-paleosol formation and underlying
109 Cretaceous sedimentary rocks are actively incised by the main stem and its tributaries (Shi and Shao, 2000; Guo et
110 al., 2002; Wang and Fu et al., 2016). Notably, the Ordos Basin underlying the CLP is rich in oil and gas (Guo et al.,
111 2014). In the lower reaches, the river drains Quaternary fluvial deposits and sedimentary rocks.

112 The Huanghe drainage basin encompasses the entire arid and semi-arid region of northern China in the upper and
113 middle reaches, and is characterized by more humid climate conditions in the lower reaches. Annual average
114 precipitation (over the period 1950 - 2000) in the upper, middle and lower reaches regions is 368 mm, 530 mm, and
115 670 mm, respectively (Wang et al., 2007). As a result of the East Asian summer and winter monsoon circulations, the
116 rainy season (June to September) contributes 85% of the annual precipitation (Wang et al., 2007). During the rainy
117 season, frequent storm events lead to concentrated flows (relatively high discharge) in vulnerable gully-hill systems,
118 the dominant regional geomorphic landscape, and actively participates in soil erosion in the CLP (Shi and Shao, 2000;
119 He et al., 2004; Qu et al., 2020). The present-day (2002 to 2016) suspended sediment flux delivered by the Huanghe
120 to the sea is about 0.12 Gt/yr, which implies a decrease of nearly 90% in sediment export compared to the widely cited
121 estimate of 1.08 Gt/yr (average value between 1950 to 1980, Milliman and Farnsworth, 2011). This massive decrease
122 in sediment export mostly results from human perturbations, including soil conservation practices in the CLP and
123 retention in large reservoirs, rather than from climatic variations such as the decreasing precipitation observed in the
124 region over the last decades (Wang et al., 2007; Ran et al., 2013; Wang and Fu et al., 2016). A scheme for water and
125 sediment regulation (WSR) has been implemented through the construction of the Xiaolangdi Reservoir since 2002,
126 aiming to mitigate water and sediment imbalances in the lower reaches. This regulation has resulted in a modification
127 of the flux of sediment delivered to the lower reaches and estuary, making the Huanghe a highly human-regulated
128 river system. However, no WSR was implemented in 2016, the year of our sampling campaign, suggesting that the
129 collected SPM samples are not significantly affected by retention in dams, and thus are representative of the fluvial
130 transport of terrestrial materials eroded from the CLP.



131
 132 Figure 1: (a) Elevation map of the Huanghe drainage basin showing the main reservoirs and gauging stations along the
 133 main stem as well as our sampling site (36.75°N, 117.02°E, near the Luokou gauging station); and (b) channel cross-section
 134 sampled for this study showing the depth and lateral distribution of suspended particulate matter (SPM) samples and
 135 modeled velocity distribution based on the "law of the wall", using the point velocity data measured by a current velocity
 136 meter attached to the sampler.

137 3 Sampling and analytical methods

138 3.1 Sampling strategy

139 Detailed sampling of a cross-section of the Huanghe was carried out on the 17th of July, 2016, during the flood season
 140 (Figure S2). Samples were collected along five depth profiles near the Luokou hydrological station, 250 km upstream
 141 from the river mouth (Figure 1). This sampling strategy allows for accessing the full range of suspended sediment
 142 particle size (Bouchez et al., 2014). The cross-section is 200-meters wide at the surface and 4 meters deep at most



143 (Figure 1). As in previous studies, we used a home-made, 10-liter, point-sediment horizontal Niskin-type sampler
144 attached to a current velocity meter, to collect river water samples and measure the water velocity simultaneously.
145 Subsequently, two water samples were collected at the surface near the right bank in May and June 2017 before the
146 flooding season, to retrieve fine suspended particulate matter. For each sample, approximately 30 liters of river water
147 were collected and were then filtered through pre-weighed 0.22- μm porosity cellulose acetate membrane filters within
148 24 hours. After rinsing the filters with filtered water, all sediment samples were transferred into centrifuge tubes and
149 freeze-dried before weighing and analysis. A bed sediment sample was collected on an exposed, recently flooded
150 sediment bar of the riverbed.

151 3.2 Physical and geochemical analysis

152 Apart from a 50-mg aliquot of SPM samples preserved for particle size analysis, samples were finely ground using an
153 agate mortar and pestle prior to chemical and isotopic analyses. The particle size distribution of the unground aliquots
154 was measured using a Laser Diffraction Particle Size Analyzer (Beckman Coulter LS-12 320) at the École Normale
155 Supérieure (ENS), Paris, France. Before analysis, unground SPM aliquots were dispersed in deionized water and then
156 in sodium hexametaphosphate in an ultrasonic bath. For each sample, we measured three replicates and report the
157 average median particle size (D_{50} , μm) with an uncertainty better than 2% (Table 1). The chemical composition of
158 SPM samples was measured on ground aliquots at the Centre de Recherches Pétrographiques et Géochimiques
159 (CRPG), Vandoeuvre-lès-Nancy, France, using inductively coupled plasma atomic emission spectroscopy (ICP-OES)
160 for major elements with typical uncertainties of 3% (Carignan et al., 2001).

161 For particulate organic carbon content (POC%, wt.), stable carbon isotope $\delta^{13}\text{C}$ (in ‰_{VPDB}, *i.e.*, in ‰ relative to Vienna
162 Pee Dee Belemnite) and radiocarbon isotope $\Delta^{14}\text{C}$ (expressed as fraction modern, Fm), ground homogenized samples
163 were fumigated using 12M HCl fumes in a closed Teflon tank at 60 °C for 48 hours to remove the carbonate fraction,
164 and were then dried under vacuum prior to analysis. Total nitrogen content (TN%, wt.) was measured on non-acidified
165 samples (Komada et al., 2008). Triplicate analysis on POC% and $\delta^{13}\text{C}$ of POC (acidified aliquots) as well as TN%
166 (non-acidified aliquots) were carried out on an Organic Elemental Analyzer (OEA) coupled with Isotope Ratio Mass
167 Spectrometry (IRMS, Thermo Scientific Flash 2000) under continuous flow mode at Géosciences Paris Saclay
168 (GEOPS), Orsay, France. Uncertainties on POC%, $\delta^{13}\text{C}$, and TN%, based on replicate measurements (1σ , $n=3$), are
169 lower than 0.02%, 0.06‰, and 0.02‰, respectively. The ^{14}C activity of POC was measured on a new compact
170 accelerator mass spectrometry (AMS), ECHoMICADAS (Hatté et al., 2016), using a gas ion source interface system
171 at the Laboratoire des Sciences du Climat et de l'Environnement (LSCE), Gif-sur-Yvette, France, with an absolute
172 uncertainty of max $\pm 0.5\%$.

173 3.3 POC source apportionment

174 To quantify the contribution and associated uncertainties of various sources to POC transported in the Huanghe, a
175 Bayesian Markov chain Monte Carlo based on a three-end member mixing scheme (burn-in of 1,000 steps, data
176 thinning of 100, and iterations of 5,000,000) was adopted (Andersson et al., 2015). This approach assumes that the
177 uncertainty on each end member contribution can be represented by a normal distribution. The mixing model was



178 constructed on the dual stable and radioactive isotope of the riverine POC pool ($\delta^{13}\text{C}$ and $\Delta^{14}\text{C}$) and of the three
179 potential source pools (section 5.2) by the following equations:

$$180 \quad \text{Isotope_ratio}_{\text{sample}} = \sum_{\text{source}} (f_{\text{source}} * \text{Isotope_ratio}_{\text{source}})$$

$$181 \quad \sum_{\text{source}} f_{\text{source}} = 1$$

182 where $\text{Isotope_ratio}_{\text{sample}}$ is either the $\delta^{13}\text{C}$ or $\Delta^{14}\text{C}$ value of the sample, $\text{Isotope_ratio}_{\text{source}}$ is either the $\delta^{13}\text{C}$ or
183 $\Delta^{14}\text{C}$ value of different possible sources of POC and f_{source} the relative contribution of each source of POC.

184 3.4 Depth-integrated fluxes

185 Instantaneous depth-integrated fluxes of SPM and POC sources were calculated for the cross-section using a method
186 developed by Bouchez et al. (2011a, b). This method is based on the systematic variation of SPM concentration in the
187 water column (Figure 2) applying a Rouse-based model (Rouse, 1937). We first constructed a bathymetric profile of
188 the river cross-section based on the depth information collected in the field and then modeled the velocity distribution
189 across the transect (Figure 1b) through fits of the so-called "law of the wall" to water velocity measured at the location
190 of each sample within the cross-section using a current meter. Afterward, the concentration of total SPM and various
191 particle size fractions could be estimated by applying the so-called Rouse model (Rouse, 1937) to each particle size
192 fraction separately (Bouchez et al., 2011a), resulting in a map of the particle size distribution in the river cross-section
193 (Figure S3). The aluminum to silicon ratio (Al/Si mass ratio) is inversely related to the particle size of river SPM in
194 the Ganges-Brahmaputra, the Amazon, and the Mackenzie Rivers (Galy et al., 2007; Bouchez et al., 2014; Hilton et
195 al., 2015). Such a linear relationship between D50 and Al/Si was also observed in our dataset, allowing for computing
196 the spatial distribution of POC content in the cross-section, based on the linear relationship between POC and Al/Si
197 (Figure 3). Finally, combining modeled water velocity, SPM concentration, and POC distribution we calculated a
198 depth-integrated, instantaneous POC flux for the whole river channel (Figure S3, detail in supplementary material).

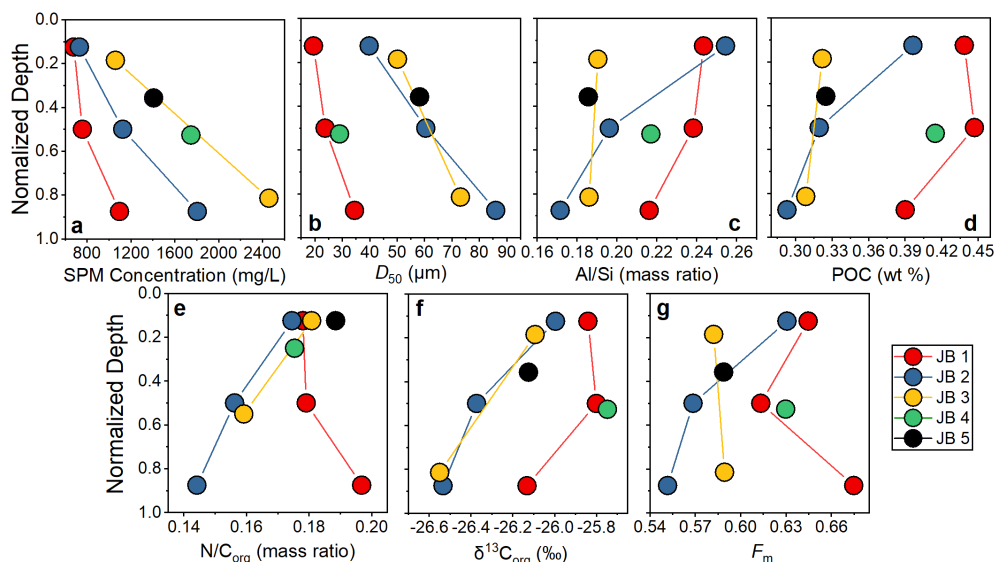
199 4 Results

200 We report the first isotopic dataset of POC samples collected along several depth profiles distributed over a cross-
201 section of the Huanghe (Table 1). SPM concentrations range from 679 to 2,459 mg/L (avg. 1,286 mg/L) and show an
202 obvious increase from the surface to the bottom and from the right bank to the left bank (Figure 1b and 2a). The
203 surface SPM concentration (*i.e.*, samples collected 0.5 m below the surface) decreases laterally as the water column
204 deepens. The range of measured Huanghe SPM D50, *i.e.* the median particle size (19.5-86.0 μm , Figure 2b) agrees
205 with that (16.6-120.1 μm) of SPM collected at Lijin during the same flooding season by Moodie et al. (2022). The
206 finest SPM is transported on the right bank and at the surface, while the coarsest SPM is found at the bottom of the
207 middle profile (sample JB 2-3). Two types of depth profiles can be distinguished at Luokou based on particle size
208 distributions (Figure S4) and the relationship between D50 and water depth (Figure 2b). On the one hand, the JB 1
209 and JB 4 profiles show a well-marked, bi-modal distribution of particle size (Figure S4) together with relatively low
210 and consistent D50 (Figure 2b). On the other hand, the JB 2, JB 3, and JB 5 profiles show a more unimodal distribution



211 of particle size (Figure S4) and a unique D50 - sampling depth relationship (Figure 2b). Interestingly, these two groups
212 can also be distinguished in terms of relationships between POC% and $\delta^{13}\text{C}$ with water depth (Figures 2d and 2f). As
213 expected, the Al/Si ratio is well-related to the particle size, with ratios of the middle profile varying from 0.17 (sample
214 JB 2-3) to 0.26 (sample JB 2-1), covering the full range of Al/Si measured in the whole cross-section (avg, $0.21 \pm$
215 0.03 , Figure 2c). The relatively low Al/Si ratios are comparable to that of the middle Huanghe (Qu et al., 2020) and
216 other large turbid river systems such as the Ganges-Brahmaputra (Galy et al., 2008b), Salween, and Irrawaddy (Tipper
217 et al., 2021).

218 SPM in the Huanghe is characterized by low TN and POC content (wt.%), ranging from 0.04% to 0.08% (avg., 0.06
219 $\pm 0.01\%$) and from 0.29% to 0.42% (avg., $0.37 \pm 0.06\%$), respectively (Figure 2d; Table 1). POC content generally
220 decreases from the surface to the river bed, with quantitative differences from one profile to another (Figure 2d).
221 Notably, the JB 1 profile shows the highest POC% and TN%. In addition, the ratio of TN% to POC%: $\text{N}/\text{C}_{\text{org}}$ increases
222 with depth in the JB 1 profile (from top to bottom), while it decreases in the JB 2 and JB 3 profiles (Figure 2e). The
223 $\delta^{13}\text{C}$ of POC varies over a narrow range from -26.55% to -25.75% (avg., $-26.12 \pm 0.29\%$, Figure 2f) and becomes
224 lighter with depth, showing that fine SPM has higher $\delta^{13}\text{C}$ than coarse SPM. These values are lower than those
225 previously reported for other Huanghe sampling sites upstream: $-24.7 \pm 0.4\%$ at Toudaoguai, $-24.9 \pm 0.6\%$ at
226 Longmen, and $-23.8 \pm 0.6\%$ at Lijin (Qu et al., 2020, Hu et al., 2015; Tao et al., 2015; Yu et al., 2019a; Ge et al.,
227 2020). The radiocarbon activity of POC of the Huanghe at Luokou is relatively low (Figure 2g), with F_m ranging
228 from 0.552 ($\Delta^{14}\text{C} = -453\%$; sample JB2-3) to 0.675 ($\Delta^{14}\text{C} = -331\%$; sample JB1-3), spanning from 3,160 to 4,780
229 ^{14}C yr, and the average value is 0.607 ± 0.038 ($\Delta^{14}\text{C} = -412\%$). This range of radiocarbon activity is consistent with
230 published values for POC collected at the river surface downstream of Toudaoguai (Qu et al., 2020). All the POC
231 radiocarbon activity data reported so far for the Huanghe are comparable to mean values for Arctic large rivers ($\Delta^{14}\text{C}$
232 $= -397\%$, ca. 4,480 ^{14}C yrs, Ke et al., 2022), revealing the multimillennial-age nature of POC transported by the
233 Huanghe. The elemental and isotopic signatures of the two fine SPM samples HH 17.05 and HH 17.06 (on average
234 $\text{POC}\% = 1.07\%$, $\delta^{13}\text{C} = -25.67\%$, $F_m = 0.720$; and $\text{Al}/\text{Si} = 0.37$) are significantly different from those of the depth
235 profile samples (Table 1). The bedload sample has a comparatively low POC% (0.21%), $\delta^{13}\text{C}$ (-27.35%), F_m (0.099),
236 and Al/Si ratio (0.17).



237

238

239

240

241

Figure 2: Variation of physical and chemical parameters in the river cross-section, shown as a function of sampling depth normalized to total depth of the water column at the location of the considered depth-profile, for the Luokou cross-section on the Huanghe (June 16, 2017). (a) SPM concentration; (b) particle size distribution (shown as D50); (c) Al/Si mass ratio; (d) POC content (weight %); (e) N/C_{org} mass ratio; (f) stable carbon isotope ratio $\delta^{13}\text{C}_{\text{org}}$ (‰); (g) radiocarbon activity F_m .

242

Table 1: SPM characteristics and POC properties of the river-cross-section sampling.

Sample ID	Type	Depth (m)	SPM mg/L	POC (%)	SD	$\delta^{13}\text{C}_{\text{org}}$ (‰)	SD	F_m	$\Delta^{14}\text{C}$ (‰)	SD	^{14}C age	TN (%)	N/C _{org}	Al/Si	D50 μm
JB 1-1	SPM	0.5	679	0.44	0.02	-25.84	0.03	0.645	-360	7	3527	0.078	0.178	0.243	19.5
JB 1-2	SPM	2	757	0.45	0.01	-25.80	0.06	0.613	-392	11	3929	0.080	0.179	0.238	23.7
JB 1-3	SPM	3.5	1095	0.39	0.01	-26.13	0.04	0.675	-331	7	3161	0.077	0.197	0.216	34.5
JB 2-1	SPM	0.5	730	0.40	0.03	-26.00	0.01	0.631	-374	7	3703	0.069	0.175	0.255	39.8
JB 2-2	SPM	2	1124	0.32	0.01	-26.37	0.06	0.569	-436	13	4537	0.050	0.156	0.196	60.4
JB 2-3	SPM	3.5	1806	0.29	0.01	-26.53	0.06	0.552	-453	38	4779	0.042	0.144	0.172	86.0
JB 3-1	SPM	0.5	1058	0.32	0.02	-26.09	0.03	0.582	-422	12	4346	0.058	0.181	0.190	50.1
JB 3-2	SPM	2.2	2459	0.31	0.02	-26.55	0.04	0.589	-415	11	4247	0.049	0.159	0.186	73.1
JB 4-1	SPM	1	1747	0.41	0.02	-25.75	0.06	0.630	-375	8	3714	0.073	0.175	0.217	29.0
JB 5-1	SPM	0.5	1406	0.32	0.01	-26.12	0.05	0.589	-416	11	4256	0.061	0.188	0.186	58.2
HH 17.05	SPM	0	83	0.92	0.00	-25.73	0.14	0.711	-295	19	2740	0.184	0.200	0.358	5.2
HH 17.06	SPM	0	54	1.21	0.01	-25.60	0.07	0.729	-277	25	2539	0.261	0.215	0.377	4.3
HH	Bedload			0.21	0.03	-27.35	0.05	0.099	-901	7	18539	0.019	0.087	0.175	44.4

243

5 Discussion

244

We observe significant heterogeneities of elemental and isotopic carbon composition as well as inorganic chemistry

245

over the studied river cross-section. The possible mechanisms behind these variations are assessed hereafter. Then,

246

sources of riverine POC are determined and quantified, confirming that erosion of the loess-paleosol sequence of the

247

CLP is a major source of aged and refractory biospheric OC to the Huanghe. Finally, we assess the POC load and its

248

variability over the transect profile, inferring the importance of the supply of POC from the river bottom in the

249

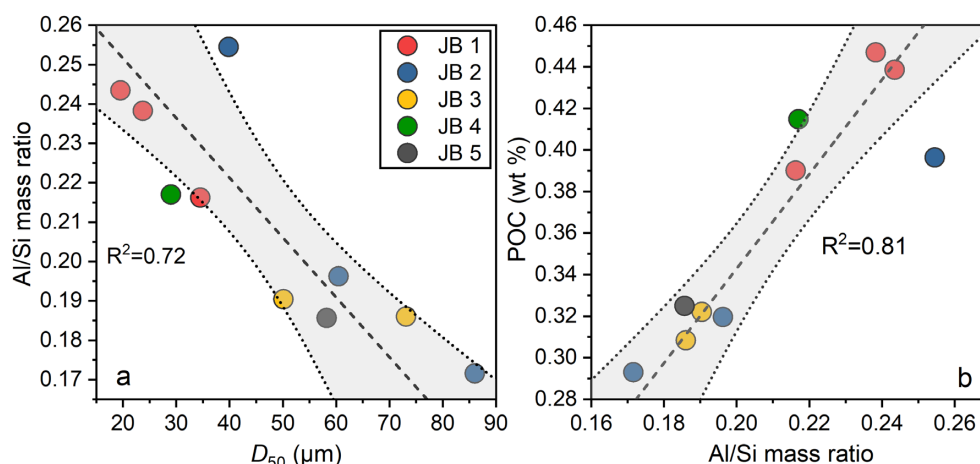
Huanghe.



250 **5.1 Transportation mode of POC in the Huanghe**

251 **5.1.1 POC loading and its controls**

252 The Huanghe is characterized by a high SPM load with relatively low POC% (avg. $0.37 \pm 0.06\%$). In the Luokou
 253 cross-section, POC content generally increases with decreasing particle size (Figure S5), with the two clay-sized
 254 ("HH") samples showing the largest POC content (Table 1). Consistently, the Al/Si ratio of Huanghe sediments, which
 255 varies as an inverse linear function of the median particle sizes D_{50} ($R^2=0.72$, Figure 3a), positively correlates with
 256 POC% ($R^2=0.81$, Figure 3b), a pattern observed globally (Galy et al., 2008b; Bouchez et al., 2014; Hilton et al., 2015).
 257 This pattern is consistent with POC variability in the Huanghe reported for manually separated size fractions of
 258 sediments (Yu et al., 2019b).

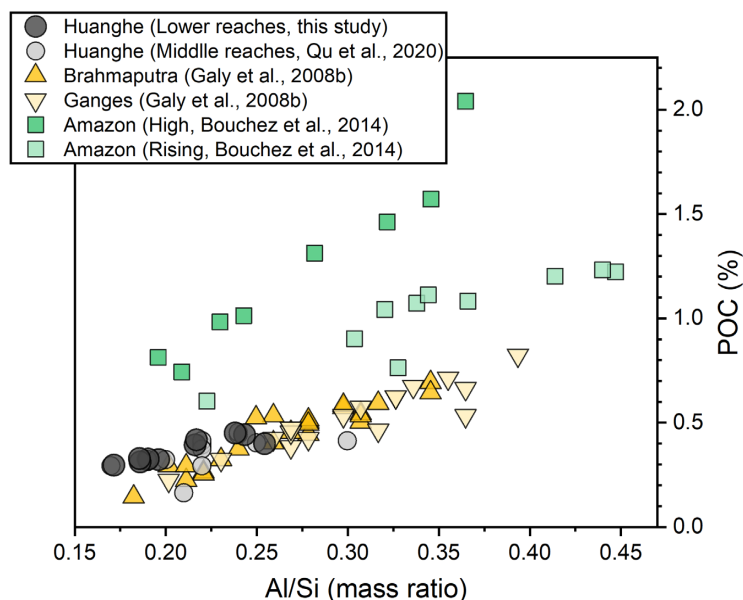


259
 260 **Figure 3: Relationships between (a) particle size D_{50} and Al/Si mass ratio; (b) Al/Si mass ratio and POC content for the**
 261 **Luokou cross-section on the Huanghe (July 17, 2016). The grey shade represents the 95% confidence area of the linear best-**
 262 **fit (black dashed line), the upper and lower bound are marked by grey dotted lines.**

263 The first reason for the low POC content of Huanghe sediments is therefore their relatively low values of Al/Si
 264 compared to other systems - a feature than can be related to the quartz-rich, OC-poor nature of the loess-paleosol
 265 formations of the CLP (Jahn et al., 2021; Huang and Ren, 2006; He et al., 2006; Ning et al., 2006; Wang and Fu,
 266 2016). However, Huanghe sediments are relatively poor in POC, even considering their low Al/Si, compared to other
 267 rivers globally. To that effect, the so-called "POC loading" can be characterized by the slope described by sediment
 268 data in an Al/Si-POC diagram (Galy et al., 2008b; Figure 4). For a given Al/Si ratio, the POC% in the Luokou cross-
 269 section is similar to that of the middle Huanghe (Qu et al., 2020), indicating the relatively invariant transport mode of
 270 POC between the middle and lower reaches. Previous studies have shown that the positive relationship between POC%
 271 and Al/Si can be partially explained by OC adsorption onto the mineral surface (Curry et al., 2007; Galy et al., 2008b;
 272 Blair and Aller, 2012; Bouchez et al., 2014; Qu et al., 2020). In the loess-paleosol deposits acting as a source of
 273 sediments to the Huanghe, OC is mostly preserved and stabilized by forming organo-aggregates with kaolinite and
 274 through adsorption onto iron oxides (Wang et al., 2013).



275 However, POC loading in the Huanghe is small compared to that of the Amazon (Bouchez et al., 2014), but similar
 276 to that of the Ganges-Brahmaputra system (Galy et al., 2008b). While many factors could influence POC loading
 277 across these catchments, we note that another similarity between the Huanghe and Ganges-Brahmaputra fluvial
 278 systems is their millennial-aged OC_{bio} (Galy et al., 2007; Tao et al., 2016). This is in stark contrast with the Amazon,
 279 where younger OC_{bio} ages have been reported (Bouchez et al., 2014). Given that younger OC_{bio} recently
 280 photosynthesized in terrestrial or aquatic ecosystems can be readily oxidized within catchments (Mayorga et al., 2005),
 281 the relatively low POC loading observed at the mouth of the Ganges-Brahmaputra and the Huanghe (Figure 4) could
 282 be related to the predominance of refractory, aged OC_{bio} and OC_{petro} in those systems, while the Amazon sediments
 283 would still contain significant amount of younger, more labile OC_{bio} .



284 **Figure 4: "POC loading" of river SPM of large rivers. The POC loading is estimated from the slope of the relationship**
 285 **between POC content and the Al/Si ratio of each fluvial system (Galy et al., 2008b). All SPM samples were collected along**
 286 **depth profiles except for the middle Huanghe (Qu et al., 2020).**
 287

288 In detail, and as explained in more detail below (**Section 5.1.2**) we also observe a significantly different POC loading
 289 between the JB 1 and JB 2 depth profiles at the Luokou station (Figure 3). This difference in POC loading in the cross-
 290 section of the Huanghe might indicate the delivery of recent OC_{bio} , specifically near the right bank (the closest to the
 291 JB 1 profile) for the Luokou site, a scenario which is supported by the comparatively younger age of POC in profile
 292 JB 1. Consistently with this interpretation, temporally variable POC loading at a given site has been reported for the
 293 Amazon (Bouchez et al., 2014), where higher POC loading during the high-water stage compared to the rising water
 294 stage has been attributed to the erosion of discrete organic debris from riverbanks.

295 Variable POC loading amongst large catchments has implications for evaluating the likelihood of POC preservation
 296 in estuaries. The Ganges-Brahmaputra system delivers relatively old, refractory OC_{bio} to the Bengal Fan with an almost
 297 complete burial efficiency (Galy et al., 2007). Given the observed similarity in POC loading and age, we can thus
 298 expect a similar, efficient preservation for the Huanghe offshore depositional system. In addition to the low reactivity



299 of the POC transported by the Huanghe, the high sediment accumulation rates in the Huanghe coastal domain might
300 further inhibit OC oxidation (Blair and Aller, 2012). Consequently, the case of the Huanghe differs drastically from
301 that of the Amazon, where higher POC loading is observed, with a larger contribution of young, labile OC_{bio} either as
302 discrete organic matter or associated with mineral surfaces, leading to low POC burial efficiency in the ocean
303 (Bouchez et al., 2014; Blair and Aller, 2012).

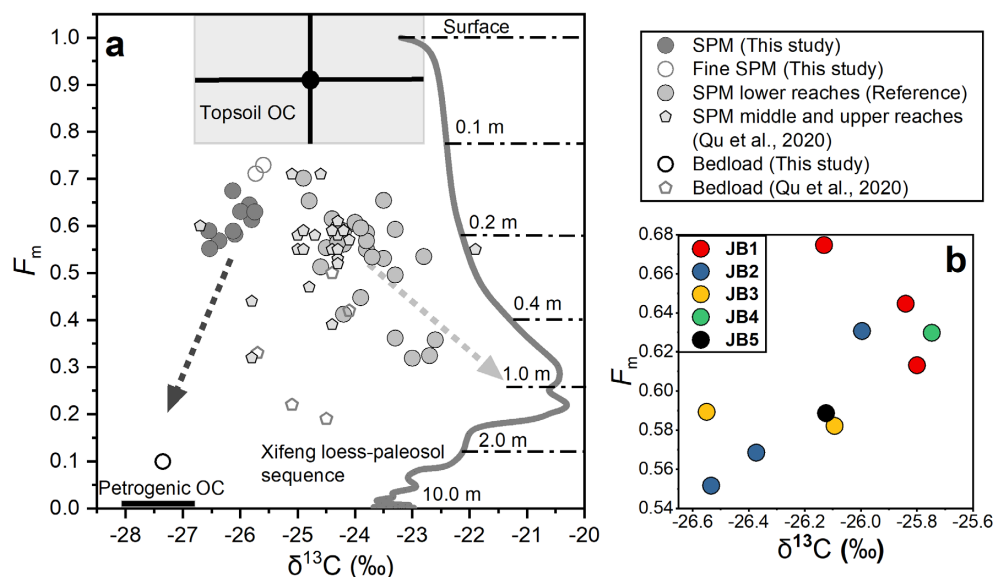
304 **5.1.2 Chemical heterogeneity within the transect**

305 There is clear lateral and vertical variability of POC content and SPM inorganic chemistry across the Luokou cross-
306 section of the Huanghe. For each vertical depth profile, clay-rich fine particles are transported near the channel surface,
307 and quartz-rich coarse particles flow near the river bottom. Accordingly, the Al/Si ratio, POC content and POC
308 radiocarbon activity generally decrease with depth. Elemental (POC%) and isotopic POC signatures (¹³C and ¹⁴C) are
309 inversely related to the particle size (D₅₀; Figure S5). These patterns are observed in other large fluvial systems, e.g.,
310 Ganges and Brahmaputra, Amazon and Mackenzie (Galy et al., 2008b; Bouchez et al., 2014, Hilton et al., 2015),
311 showing that hydrodynamic sorting is the primary control on suspended sediment OC content, segregating inorganic
312 and organic material according to particle size (Bouchez et al., 2011a, 2014).

313 At the Luokou sampling site, lateral variability at the channel surface shows that POC-rich fine particles are
314 preferentially transported near the right bank (Figure 2 and Figure S3). The channel geometry thus needs to be
315 examined as a potential factor to produce such lateral heterogeneity, in particular through bank erosion and bedload
316 resuspension.

317 Bank erosion can be a significant mechanism for the delivery of sediments to river systems (Guo et al, 2007). Bank
318 erosion at Luokou would make OC from the lower Huanghe alluvial plain a potential source of POC in the lower
319 reaches of the Huanghe. This mechanism provides a possible explanation for the opposite trends displayed by samples
320 from the JB 1 and JB 2 profiles in the Fm vs. δ¹³C space (Figure 5). The youngest POC was found at the bottom of
321 the JB 1 profile. Meanwhile, the JB 1 samples have comparatively higher N/C_{org} ratios and N%, consistent with the
322 input of discrete organic matter (e.g., plant debris) from the bank in addition to rock-derived detrital clastic material
323 in the coarse fractions (> 32 μm, Yu et al., 2019b). Such input would also provide an explanation for the higher POC
324 loading of the JB 1 profile (**Section 5.1.1**).

325 Resuspension of bed sediments is also a possible mechanism to explain the lateral heterogeneity in POC content in
326 the study cross-section of the Huanghe. Indeed, scouring of channel bed sediment at high water flow may also shift
327 POC to more negative radiocarbon and stable isotope signatures. Our sample set collected in July 2016 during flooding
328 (water flow velocity up to 2.1 m/s, Figure 1) supports this scenario. Indeed, the increase in D₅₀ of surface SPM
329 samples from right to the left bank, that is with total channel depth decrease, is consistent with coarse sediment
330 resuspension from the bed. Such a scenario is also supported by the three-fold increase in sediment flux observed
331 along the course of the Huanghe from Huayuankou to Lijin in July 2016, despite a four-fold decrease in water
332 discharge (Figure S2).



333
 334 **Figure 5: (a) ^{14}C activity (expressed as F_m) vs. $\delta^{13}C$ for a compilation of POC data collected over the 2011-2016 period in**
 335 **the lower Huanghe, including samples from this study and previous studies at Huayuankou, Lijin, and Kenli (Hu et al.,**
 336 **2015; Tao et al., 2015; Yu et al., 2019a; and Ge et al., 2020); SPM and bedload collected by Qu et al., 2020 at Toudaoguai**
 337 **(most downstream location of the upper reaches) and Longmen in the middle reaches (Table S1). The grey curve**
 338 **corresponds to $\delta^{13}C_{org}$ of the top 10 m of the Xifeng loess-paleosol (Ning et al., 2006), and the corresponding F_m was**
 339 **calculated from ^{10}Be -derived ages following ‘Age = $-8033 \cdot \ln(F_m)$ ’. The soil depth is marked above the dot-dash line (Zhou**
 340 **et al., 2010). Topsoil OC represents OC from the upper 10 cm of the loess-paleosol sequence with standard deviation marked**
 341 **with black lines. (b) ^{14}C activity (expressed as F_m) vs. $\delta^{13}C$ diagram for the Huanghe sediment samples collected in this**
 342 **study at the Luokou cross-section.**

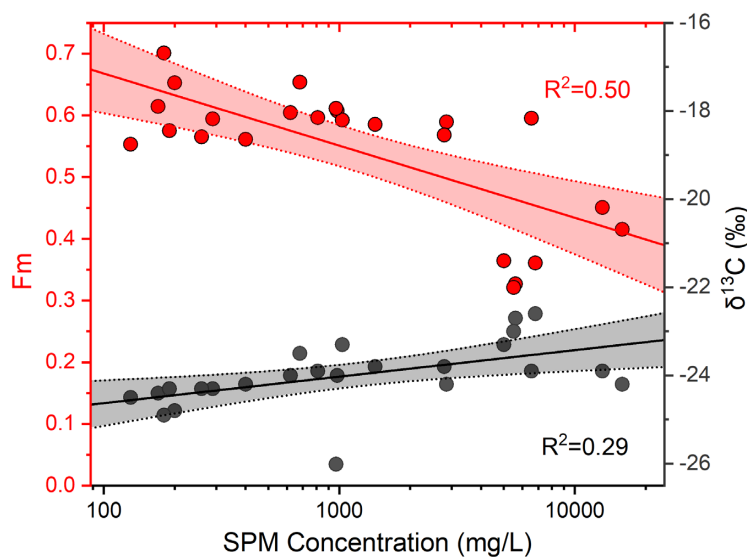
343 5.2 POC provenance in the Huanghe: the significance of loess-paleosol-derived OC

344 5.2.1 Physical erosion of the loess-paleosol sequence

345 Over decennial to centennial time scales, the POC export of the Huanghe is mainly controlled by erosion of the CLP.
 346 Throughout the Quaternary, the erosion rate in the Huanghe basin has been mainly driven by climate shifts until human
 347 activities started and profoundly impacted sediment fluxes in the mid-Holocene (He et al., 2006). To determine the
 348 contributions of the various terrestrial OC components to Huanghe POC, we compiled published POC carbon isotope
 349 data for sediments collected in the lower reaches from 2011 to 2016 (Figures 5 and 6). Even though the Huanghe has
 350 experienced a 90% decrease in annual sediment load since the 1950s (Wang et al., 2015), the radiocarbon ages of
 351 Huanghe POC are considerably old (avg $5,100 \pm 1,700$ ^{14}C yr, $n=29$), with a minor fraction of modern
 352 photosynthesized OC_{bio} (Tao et al., 2015; Yu et al., 2019a, b). This relatively ^{14}C -depleted POC suggests the significant
 353 contribution of OC originated from deep soil horizons within the catchment. Given the fact that loess is easily erodible,
 354 the negative trend between ^{13}C and F_m of POC for sediment samples collected in the Huanghe over the 2011-2016
 355 period (Figure 5a) suggests that deep horizons of loess-paleosol formations are a plausible source for the ^{14}C -depleted
 356 end member. Besides, the preferential erosion of recently photosynthesized and possibly degraded OC_{bio} from the
 357 overlying topsoils (< 10 cm) most likely contributes to riverine POC (Tao et al., 2015).



358 As such, variable contribution of aged and radiocarbon-free OC from deep horizons of loess-paleosol formations of
 359 the CLP should have a significant impact on the elemental and isotopic signature of POC in the lower Huanghe.
 360 Erosion of loess-paleosol can also explain the decreasing POC% with increasing SPM concentration at different sites
 361 of the main channel (Ran et al., 2013; Qu et al., 2020), the negative relationship between SPM concentration and
 362 corresponding POC Fm at Luokou (Figure 6), and the low POC loading of the Huanghe (Section 5.1.1), as the deep
 363 horizons of the loess-paleosol sequences are OC-poor, and mostly host OC that is highly degraded and refractory (Liu
 364 et al., 2012; Wang et al., 2013; Cheng et al., 2020). However, the slight increase of POC $\delta^{13}\text{C}$ with increasing SPM
 365 concentration might indicate a significant supply of soil OC from loess-paleosol shallower depth, as inferred from the
 366 $\delta^{13}\text{C}$ variation within the Xifeng loess-paleosol sequence (Figure 5a).



367
 368 **Figure 6:** ^{14}C activity (expressed as Fm; red circles) and $\delta^{13}\text{C}$ (black circles) of POC vs. SPM concentration for surface
 369 samples from the Huanghe collected from 2011 to 2016 (average SPM concentration of surface samples in this study and
 370 from Hu et al. (2015), Tao et al. (2015), Yu et al. (2019a), and Ge et al. (2020)). These paired dual carbon isotope data
 371 corresponds to the group ‘SPM lower reaches’ in Figure 5. Straight lines correspond to best-fit logarithmic curves, and
 372 shaded areas represent the 95% confidence interval.

373 The $\text{N}/\text{C}_{\text{org}}$ ratio provides additional evidence for the significant contribution of loess-paleosol material to Huanghe
 374 POC (Figure S6). Indeed, the $\text{N}/\text{C}_{\text{org}}$ ratios of SPM collected in the lower reaches ranges from 0.10 to 0.23 (this study,
 375 Ran et al., 2013; Yu et al., 2019a), whereas topsoils of the CLP are characterized by $\text{N}/\text{C}_{\text{org}}$ lower than 0.14 (Liu and
 376 Liu, 2017) and sedimentary rocks typically have very low $\text{N}/\text{C}_{\text{org}}$ (Hilton et al., 2015). Soil OC input from the North
 377 China Plain is also unlikely given its $\text{N}/\text{C}_{\text{org}}$ of 0.10-0.13 (Shi et al., 2017). Therefore, all these possible sources cannot
 378 explain the high $\text{N}/\text{C}_{\text{org}}$ signatures of riverine SPM. In addition, the high turbidity of the Huanghe ($> 600 \text{ mg/L}$) during
 379 the sampling season is likely to inhibit *in-situ* primary production ($\text{N}/\text{C}_{\text{org}} > 0.13$) (Zhang et al., 2013; Hu et al., 2015).
 380 As a result, only soil OC from deep loess-paleosol horizons appears as a plausible supplier to downstream Huanghe
 381 POC, given the high $\text{N}/\text{C}_{\text{org}}$ ratios previously reported for various loess-paleosol sequences (Figure S6, Ning et al.,
 382 2006).



383 Geomorphic processes in the CLP region support the erosion of deep soil horizons. There, gully erosion is thought to
384 be responsible for more than 80% of the total sediment yield in the CLP (He et al., 2006). Gullies are densely
385 distributed and cover about 42% of the total area of the CLP and up to 60% in hilly regions (Huang and Ren, 2006;
386 He et al., 2006). Nowadays, the well-developed gully geomorphic system of the CLP is characterized by gullies with
387 a depth of about 10 m on average and represents the most active vertical and regressive erosion of loess (Huang and
388 Ren, 2006). This incision process erodes all types of unconsolidated materials, including the loess-paleosol sequence,
389 underlying red clays, and colluvial deposits in the form of creeps, falls, and slides in the watershed (Zhu, 2012). All
390 these observations suggest that gully erosion strongly impacts the composition of riverine POC. As gully erosion is
391 sensitive to climate change and anthropogenic activities, soil dynamics in the Huanghe basin have been altered since
392 the mid-Holocene. In recent years, soil and water conservation and environmental rehabilitation campaigns (Wang et
393 al., 2007) largely contributed to the reduction of SPM export by the Huanghe with a transfer to the estuary of 10.6 Mt
394 in 2016, which represents a few percent of the annual sediment flux measured in 2013 (172.8 Mt) and less than one
395 percent of the flux of the 1950s (*ca.* 1,340 Mt; Wang et al., 2015). Such modifications should thus have drastically
396 inhibited the POC export by the Huanghe.

397 **5.2.2 POC source determination and end member apportionment**

398 Considering the SPM geochemistry and the basin characteristics, three terrestrial sources can be identified as necessary
399 to form the composition of the Huanghe POC at the Luokou cross-section. As discussed in **Section 5.2.1** and shown
400 in Figure 5a, two of these sources are (a) topsoil-derived OC (OC_{ts}) and (b) OC from deeper horizons of the loess-
401 paleosol sequence (OC_{lps}) excluding topsoil. In addition, at the Luokou cross-section, bed OC shows lower F_m and
402 $\delta^{13}C$ values compared to that of SPM, suggesting a significant contribution of (c) rock-derived OC from erosion in the
403 middle reaches (OC_{petro}).

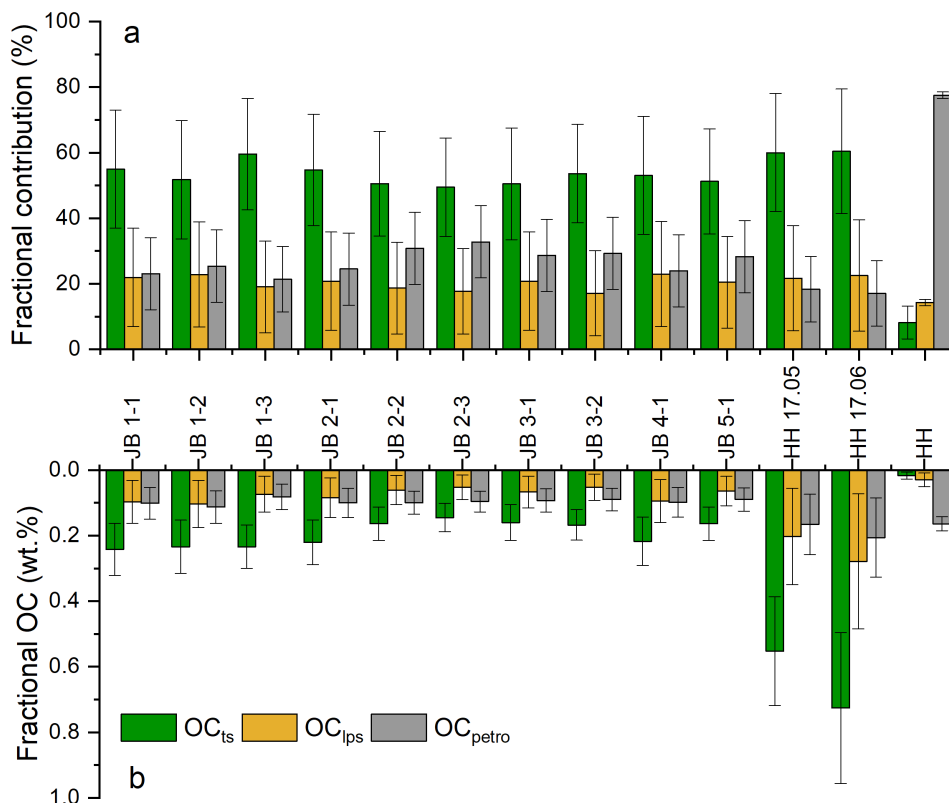
404 We adopted a Bayesian Monte-Carlo model to reconstruct source apportionment based on the mass balance of carbon
405 isotopes ($\delta^{13}C$ and $\Delta^{14}C$) of our three defined end members (**Section 3.3, Appendix A**). Modeling results are shown
406 in Figure 7 as relative contributions (Figure 7a) and weight percentage (Figure 7b) of OC_{ts} , OC_{lps} , and OC_{petro} (Table
407 S2). The contribution of OC_{petro} to total Huanghe POC at Luokou varies between 21% and 33% in the cross-section,
408 which is higher than the contribution calculated for in the two fine SPM samples (17% on average) and much smaller
409 than for the bed sediment sample ($78 \pm 10\%$). The inferred OC_{petro} concentration in the sediment is remarkably uniform
410 in the cross-section, representing $0.10 \pm 0.01\%$ of SPM (Figure 7b). This result is consistent with the OC contents of
411 midstream sedimentary rocks at $0.09 \pm 0.08\%$ (Qu et al., 2020). In addition, these findings imply that OC_{petro}
412 concentration does not depend on particle size and confirm previous findings of OC_{petro} being present in a range of
413 clastic particles or as discrete particles (Galy et al., 2008a; Bouchez et al., 2014). In other words, the rock-derived OC
414 has a relatively invariant contribution with depth (Galy et al., 2008a; Bouchez et al., 2014), meaning that biospheric
415 OC exerts a first-order control on POC content and isotopic variations throughout the cross-section.

416 At the study cross-section, OC_{ts} and OC_{lps} contribute 50%-60% and 17%-23% to the total POC, respectively (Figure
417 7a). The sum of these two components can be considered as OC_{bio} , which varies between 67% and 77%. The
418 corresponding OC_{bio} content of sediment is quite variable, ranging from 0.20% (sample JB 2-3) to 0.34% (sample JB



419 1-1), and generally decreases from the river surface to the bottom. Given the rather invariant OC_{petro} concentration in
 420 the sediment, there are thus marked heterogeneities of POC provenance in the cross-section. For instance, POC
 421 transported close to the right bank and in the finer SPM samples show a higher contribution from OC_{bio} . From the
 422 knowledge of the relative contributions of OC_{ts} and OC_{lps} and their corresponding ^{14}C activity, the F_m values for the
 423 bulk OC_{bio} can be estimated based on mass balance. The modeled radiocarbon activity of OC_{bio} is relatively
 424 homogeneous with an average $\Delta^{14}C$ value of $-178 \pm 11\text{‰}$ ($1,510 \pm 110$ ^{14}C yr) whereas a greater variance is observed
 425 in the bulk ^{14}C content. In summary, our results support the first-order control of OC_{bio} abundance on POC content
 426 and age in the Huanghe.

427



428

429

430

431

432

Figure 7: (a) Relative contributions of the three different sources of Huanghe POC, (b) fractional OC weight percentage Huanghe POC at the Luokou cross-section, as inferred from a mixing model. OC_{ts} is the topsoil-derived OC, OC_{lps} represents the loess-paleosol sequence OC excluding topsoil, and OC_{petro} is the rock-derived OC eroded from the Huanghe middle reaches.

433

434

435

436

437

Applying the same mixing model to previously published Huanghe POC data (2011-2016, Table S1) shows (1) dominance of the OC_{bio} contribution to POC, (2) variable relative mixing proportions of OC_{ts} and OC_{lps} ; (3) a wide range of ^{14}C age for OC_{bio} (from 1,040 to 8,050 yr). In particular, OC_{ts} and OC_{lps} contributed 20%-30% and 46%-68% to POC collected in 2013 (Hu et al., 2015), leading to 75-89% of OC_{bio} . Yu et al. (2019a) estimated that OC_{bio} contributed 63%-81% to the lower Huanghe POC (2015-2016) using a different mixing model. Using their data in our



438 mixing model results in a slightly higher OC_{bio} contribution of 77%-87%, consisting of 39%-53% for OC_{is} and 30%-
439 47% for OC_{lps} . The small difference in source contribution mainly results from the fact that old OC_{bio} from loess-
440 paleosol sequences was not considered in Yu et al. (2019a), and from the different isotopic signatures chosen for the
441 POC endmembers. However, both estimates ignore the possible presence of rock-derived OC in soils. In any case, our
442 results suggest that the Huanghe transports more OC_{bio} -derived POC than previously thought, with more aged, soil-
443 derived OC.

444 It is worth noticing that these calculations suggest that the OC_{lps} fraction in the Huanghe was significantly higher in
445 2013 than in 2016. As most Huanghe sediments are derived from the CLP, higher physical erosion in the CLP should
446 enhance supply of aged, refractory OC_{bio} to the river system. As a consequence, the decrease in sediment supply from
447 the CLP initiated a few decades ago (Wang and Fu et al., 2016), which is likely to continue in the future, will probably
448 lead to the reduction of the contribution of OC_{lps} to total POC export from the Huanghe. This might have an impact
449 on the burial efficiency of riverine POC on the continental margins, as OC_{is} is more labile than OC_{lps} , and thus more
450 prone to the remineralization process before burial. Moreover, decreasing erosion rate in the Huanghe basin will lead
451 to decreasing sediment accumulation rate in the estuary, which potentially favors the oxidation of all POC components
452 before burial (Blair and Aller, 2012). The time scale over which such effect could take place is yet unknown, as
453 anthropogenic intervention is the primary reason for the sediment yield reduction, through afforestation and soil and
454 water conservation measures in the CLP and reservoir operation in the middle reaches of the Huanghe. However, it is
455 plausible that in response to decreased terrestrial physical erosion on the Loess Plateau over at least decadal timescales,
456 an increased proportion of Huanghe POC will be oxidized before burial in the ocean, thereby leading to a weakened
457 preservation efficiency for the terrestrial eroded POC.

458 **5.3 POC export by the Huanghe**

459 In the Huanghe, POC content varies both vertically and laterally throughout the cross-section (Figure 2). This spatial
460 variability of both physical and chemical SPM characteristics must be considered when estimating integrated
461 instantaneous POC concentration and flux (Section 3.4).

462 We calculate that (Text S1) at the sampling time (July 2016), the Huanghe at Luokou transported 1,075 kg/s of SPM
463 for a water discharge of 731 m³/s, such that the spatially-integrated SPM concentration over the cross section (SPM_{int})
464 was 1,472 mg/L, a value relatively close to the straightforward average concentration of our 10 samples (1,286 mg/L).
465 The Luokou gauging station records a monthly SPM load of 1,826 kg/s in July 2016, and the daily average SPM load
466 of 1,096 kg/s for a daily average water discharge of 643 m³/s on the 16th and 17th of July 2016 (method: three water
467 samples collected at 0.5 m below the channel surface across the transect profile, data available at
468 <http://www.yrcc.gov.cn>). Even though the latter estimate neglects the vertical heterogeneity within this relatively
469 shallow river (< 5.0 m), estimates give similar results.

470 We further obtain an instantaneous POC flux of 3.69 kg/s, corresponding to a cross-section integrated average POC
471 content ($POC_{int}\%$) of 0.34% when dividing this instantaneous POC flux by the instantaneous SPM load. Given the
472 relatively homogenous distribution of OC_{petro} , the instantaneous flux of OC_{petro} was calculated by multiplying the
473 average OC_{petro} content by the instantaneous cross-section integrated SPM flux, yielding 1.07 ± 0.11 kg/s. The



474 instantaneous OC_{bio} flux was then calculated by subtracting the instantaneous flux of OC_{petro} from the instantaneous
475 POC flux, yielding 2.61 ± 0.26 kg/s. Assuming that our SPM samples are representative in terms of POC content
476 exported in July 2016, and taking the SPM flux of the gauging station for July, then the estimated fluxes of POC,
477 OC_{bio} , and OC_{petro} for the flood period of July 2016 are 6.1, 4.3, and 1.8 kg/s, respectively. Taking POC_{int} content for
478 estimating the annual POC flux yields a value of 1.1 kg/s consisting of 0.8 and 0.3 kg/s for OC_{bio} and OC_{petro} fluxes,
479 respectively. Note that these numbers are lower-bound estimates because POC content in Huanghe SPM collected
480 during flood periods is generally the lowest (Ran et al., 2013).

481 The above numbers present a sharp decrease compared to the estimated POC and OC_{bio} fluxes transported by the
482 Huanghe over the period 2008 to 2013. Galy et al. (2015) estimated an OC_{petro} flux of 1.9 kg/s and an OC_{bio} flux of
483 11.4 kg/s from 2008 to 2012 (SPM flux: 3,655 kg/s, YRCC 2016), while Tao et al. (2018) reported an OC_{petro} flux of
484 5.8 kg/s and a similar OC_{bio} flux of 12.6 kg/s from June 2012 to May 2013 (SPM flux: 5,723 kg/s, YRCC 2016).

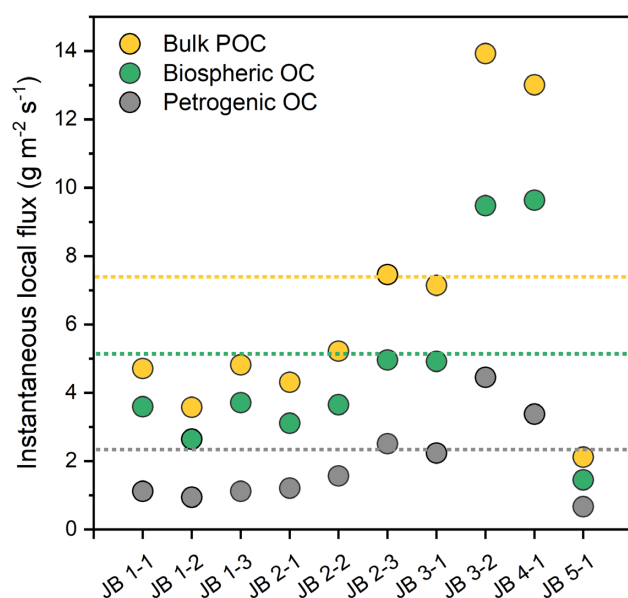
485 We first note that previous estimates of POC flux in the Huanghe might be biased as these estimates neglect the
486 variability over the cross-section (e.g., Hu et al., 2015; Ran et al., 2013; Tao et al., 2015), SPM samples analyzed so
487 far for the Huanghe were generally collected within the first 0.5 m below the surface, meaning that previous POC
488 estimates did not consider the observed vertical and lateral POC heterogeneities and have thus misestimated POC
489 sources and fluxes. Those estimates were calculated by multiplying an individual surface POC content by the
490 corresponding monthly or weekly suspended sediment load, as provided by hydrological stations. Such estimates can
491 be problematic because POC content in SPM generally decreases from top to bottom (Figure 2), resulting in biased
492 surface-based estimates of fluxes (Bouchez et al., 2014). Using our cross-section data, we can estimate the bias in
493 POC flux estimates when a single sample is used for such flux estimates, by multiplying depth-integrated sediment
494 flux by the POC content of each sample. Such calculation shows different POC fluxes ranging from -15% to $+30\%$
495 compared to the depth-integrated estimate, which is mostly influenced by the variable POC content. Considering SPM
496 collected at the channel surface, POC flux estimates using samples JB 1-1 and JB 2-1 are 28% and 15% higher,
497 respectively, and are 6% and 5% lower using samples JB 3-1 and JB 5-1, respectively, than the depth-integrated
498 estimate. This simple sensitivity analysis shows that channel surface sampling of SPM alone does not necessarily
499 result in an overestimation of POC flux because of lateral heterogeneity, even though the POC content of SPM is
500 generally higher at the surface than at the bottom (Figure 2). As a consequence, and although accurate estimation of
501 POC fluxes requires grain-size variations to be accounted for, the corresponding bias cannot explain the large
502 difference between our estimates of Huanghe POC export for the year 2016 and previous estimates for preceding
503 years. The dramatic decrease in sediment load of the Huanghe (Wang and Fu et al., 2016) has most likely exerted a
504 first-order control on the reduction in POC export from the Huanghe river system, and will probably continue to do
505 so in the near future.

506 In the lower Huanghe, the POC content is very low and has small variance among different size fractions (Get et al.,
507 2020), such that the POC flux is controlled by the SPM flux. In particular, it is worth noting that the Huanghe displays
508 strong density stratification effects compared to other rivers (Moodie et al., 2022), with near-bed flow dominating the
509 transport of SPM. In order to appraise how spatial and temporal variability in SPM flux could influence POC export,
510 "local" POC loads can be calculated throughout the cross-section using the local water velocity, SPM concentration,



511 and POC content (Figure 8). In general, in the lower Huanghe more POC is transported near the riverbed and above
 512 shallower bathymetry on the left side of the channel (except for profile JB 5). For instance, there is a nearly two-fold
 513 increase in POC export from the surface to the bottom for the JB 2 and JB 3 profiles. The maximum local bulk POC
 514 export (sample JB 3-2), OC_{bio} (sample JB 3-2), and OC_{petro} (sample JB 4-1) are over 6 times higher than the
 515 corresponding minimum values (sample JB 5-1). This spatial pattern of POC load is almost the reverse of the POC%
 516 variation over the cross-section, again stressing the importance of sediment river dynamics in POC delivery. From
 517 these considerations, it could be anticipated that during the low-water season, when water velocity is slower, near-
 518 bottom Huanghe SPM is deposited on the channel bed, withdrawing a significant fraction of the POC export, as shown
 519 in other large rivers (Ke et al., 2022). This topic should be further examined in future research, in order to
 520 systematically investigate the stratification of sediment and associated OC transport dynamics in lowland and high-
 521 turbidity fluvial systems.

522



523

524 **Figure 8: Estimates of instantaneous “local” fluxes of Huanghe bulk POC, OC_{bio} and OC_{petro} , calculated for each sample of**
 525 **the Luokou cross-section. The three dotted lines marked in orange, green, and grey represent the corresponding**
 526 **instantaneous, cross-section integrated fluxes.**

527 Interestingly, anthropogenic activities may have antagonistic effects on POC export. Deforestation, agriculture, and
 528 mining have considerably enhanced the sediment yield from the CLP since the mid-Holocene (He et al., 2006) while
 529 the construction of large dams, soil and water conservation measures, and afforestation has considerably reduced the
 530 sediment yield since the 1950s (Wang and Fu et al., 2016; Wang et al., 2007; Syvitski et al., 2005). Yet the Huanghe
 531 exports substantial OC_{bio} and OC_{petro} with a significantly higher burial efficiency (~42% on average; Sun et al., 2018)
 532 than other large fluvial systems entering passive continental margins, such as the Changjiang, Amazon, and
 533 Mississippi (Blair and Aller, 2012). It is reported that aged soil OC is nearly fully preserved in continental margins
 534 and that OC_{petro} has a *ca.* 70% burial efficiency (Tao et al., 2016). However, the contribution of the Huanghe OC burial



535 to the global C sink is likely to be lower in the future as the consequence of 1) sharp decrease in SPM and POC export
536 due to weakened physical erosion in the CLP; 2) reduced sediment accumulation rate favoring OC remineralization
537 in estuaries (Blair and Aller, 2012; Walling and Fan, 2003; Milliman and Farnsworth, 2011; Galy et al., 2015).

538 **6 Conclusions**

539 In this contribution, we present the first detailed study of particulate organic carbon (POC) over a complete river cross-
540 section of the Huanghe, providing new perspectives on the transport mode, source, and instantaneous fluxes of POC
541 in this highly turbid large river.

542 At the scale of a cross-section, physical and chemical properties of SPM are heterogeneous both vertically and
543 laterally, a feature that is mainly controlled by bathymetry and hydrodynamic sorting. Resuspension of bed sediment
544 and local erosion of the right bank together impact the suspended POC composition at the sampled location. This
545 spatial heterogeneity shows that near-bottom SPM plays a dominant role in the delivery of OC_{bio} (topsoil and deep
546 soil OC combined) and OC_{petro}. Despite a relatively shallow river channel (< 5.0 m) and narrow width (< 200 m), we
547 show how the heterogeneity of POC transport over a cross-section needs to be considered in constraining POC
548 transport mode and estimating POC fluxes.

549 Despite its millennial age, POC in the Huanghe is dominated by OC_{bio} with a contribution of from 67% to 79%. OC_{petro}
550 content in SPM is relatively homogeneous (0.08% - 0.11%) over the cross-section, indicating that the variability in
551 bulk POC age is mainly controlled by the variability in OC_{bio} content, especially in the finest SPM fraction. OC_{bio} ages
552 deduced from the application of a mixing model to previously published data (record period 2011-2016) are highly
553 variable, ranging from 1,040 to 8,050 ¹⁴C yr. We interpret this feature as resulting from the erosion of deep horizons
554 by gully systems in the loess-paleosol sequences containing ¹⁴C-dead OC_{bio}. Enhanced erosion of deep loess-paleosol
555 horizons mobilizes aged and refractory OC to the ocean, with high burial efficiency on the passive margin. The erosion
556 of loess-paleosol horizons is thus an efficient process of CO₂ burial. However, the construction of large dams has
557 drastically affected the sediment load of the Huanghe system and retains substantial quantities of sediments that were
558 previously exported to the ocean. Future work is needed to further quantify how these anthropogenic modifications
559 alter POC composition and transport, by conducting comprehensive cross-section sampling campaigns over extended
560 time series upstream and downstream from dams.

561 **Appendix A**

562 Fluvial POC delivered in the Huanghe POC could originate from three terrestrial sources. As topsoil typically contains
563 recently photosynthesized OC_{bio}, we used a $\delta^{13}\text{C}$ value of $-24.8 \pm 1.9\text{‰}$ (n=166) according to the subsurface soil OC
564 values measured across the Huanghe basin (Rao et al., 2017). Over the sampled cross-section, the depleted ¹³C values
565 indicate the dominant and almost exclusive input of C3 plant-derived material to the Huanghe POC in the lower
566 reaches. Based on ¹⁴C (Liu et al., 2012) and ¹⁰Be (Zhou et al., 2010) dating of < 10 cm-deep soil horizons in the
567 Huanghe Basin, the average age of topsoil was chosen as being younger than 2,000 yr (*i.e.*, $\Delta^{14}\text{C} > -220\text{‰}$). As the
568 topsoil end member includes modern biospheric material ($\Delta^{14}\text{C}$ around 40‰, Hua et al., 2013), we assigned a $\Delta^{14}\text{C}$



569 value of $-90 \pm 130\%$ ($F_m = 0.91 \pm 0.13$) to this endmember. This range also includes the range of $\Delta^{14}\text{C}$ values of pre-
570 aged soil OC indicated by the long-chain $n\text{-C}_{24+26+28}$ alkanols of the Huanghe POC reported by Tao et al. (2015) and
571 Yu et al. (2019a). Their results show consistent POC $\Delta^{14}\text{C}$ values in the lower reaches of $-204 \pm 20\%$ ($F_m = 0.80 \pm$
572 0.03 , $n=7$) from June 2015 to May 2016 and $-219 \pm 33\%$ ($F_m = 0.79 \pm 0.04$, $n=4$) at Kenli and of $-198 \pm 15\%$ ($F_m =$
573 0.81 ± 0.02 , $n=6$) from June 2015 to April 2016 at Huayuankou.

574 The second end member should be characterized by aged and refractory OC from the loess-paleosol sequence
575 excluding topsoil (upper 10 m) of the CLP. Radiocarbon dating has an upper age limit of around 50,000 yr, age above
576 which F_m is equal to 0. However, radiocarbon-free OC spanning from 50,000 to 100,000 yr must still be considered
577 as OC_{bio} in the long-term carbon cycle. Here, we name this ignored OC as the “dormant” OC, without which the OC_{bio}
578 (*i.e.*, less than 100,000 yr old) would be underestimated to some extent because the radiocarbon-free OC would be
579 misinterpreted as having a petrogenic origin. To consider this “dormant” OC, a $\delta^{13}\text{C}$ values of $-22.7 \pm 1.0\%$ and a
580 $\Delta^{14}\text{C}$ values of $-610 \pm 390\%$ ($F_m, 0.39 \pm 0.39$) were adopted based on an average of values over the whole loess-
581 paleosol sequence. Although radiocarbon-free (*i.e.*, older than 100,000 yr) OC overlaps with this endmember, such
582 old soil organic carbon is probably not mobilized as modern gully erosion mainly concerns the upper 10 m of the
583 loess-paleosol sequences, where soil OC_{bio} is assumed to be significantly younger comparatively (Figure 5).

584 Rock-derived OC from the QTP and the CLP, as well as kerogen from oil-gas fields from the Ordos Basin,
585 were all considered to be possible contributors to the OC_{petro} endmember. The $\delta^{13}\text{C}$ of OC_{petro} greatly varies between
586 the QTP ($-21.2 \pm 1.2\%$, $n=11$, Liu et al., 2007) and the CLP ($-26.8 \pm 0.5\%$, $n=8$, Qu et al., 2020). However, most of
587 the sediments eroded from the QTP are not transferred to the lower reaches as they remain trapped in the CLP and the
588 western Mu Us desert (Nie et al., 2015; Licht et al., 2016; Pan et al., 2016). In addition, the construction of large dams
589 in the upper reaches has considerably reduced the transfer of solid materials downstream (Wang et al., 2007).
590 Therefore, rock-derived OC inherited from the denudation of the QTP region is not further considered. Kerogen from
591 the oil-gas fields of the Ordos Basin in the CLP region (Figure 1) has $\delta^{13}\text{C}$ values of $-29.2 \pm 0.9\%$ ($n=10$, Guo et al.,
592 2014). Taking these constraints together, we consider a $\delta^{13}\text{C}$ value of $-28.1 \pm 1.5\%$ for the OC_{petro} end member, and
593 a $\Delta^{14}\text{C}$ value of -1000% ($F_m = 0$) by definition.

594 **Data availability**

595 All datasets are included in the paper and the supplementary materials.

596 **Author contributions**

597 DC, JB, CQ, and YK conceptualized the study. DC, JB, YK, MM, and BC determined the methodology. HC and JC
598 collected the sediment samples. YK, MM, and AN assisted with elemental and isotopic carbon analysis. DC and CQ
599 supervised the work. KY performed data analysis and wrote the original draft, and all authors contributed to the review
600 and editing of the paper.



601 **Competing interests**

602 We declare there is no competing interest.

603 **Acknowledgments**

604 We thank Yulong Liu and Shengliu Yuan for their help during sampling and filtering. We also thank François Thil
605 and Nadine Tissenerat for invaluable help when running the ECHOMICADAS, and Pierre Barré for use of the
606 Beckman Coulter's LS 13 320 for particle size analysis at École normale supérieure.

607 **Financial support**

608 This study was financially supported by the Agence Nationale de la Recherche (ANR) SEDIMAN (Grant ANR-15-
609 CE01-0012), the National Natural Science Foundation of China (NSFC), grants 41561134017, 41625012, and the
610 China Scholarship Council (CSC) to Yutian Ke (No.201706180008).

611 **References**

- 612 Andersson, A., Deng, J., Du, K., Zheng, M., Yan, C., Sköld, M., and Gustafsson, Ö.: Regionally-Varying Combustion
613 Sources of the January 2013 Severe Haze Events over Eastern China, *Environ. Sci. Technol.*, 49, 2038–2043,
614 <https://doi.org/10.1021/es503855e>, 2015.
- 615 Baronas, J. J., Stevenson, E. I., Hackney, C. R., Darby, S. E., Bickle, M. J., Hilton, R. G., Larkin, C. S., Parsons, D.
616 R., Myo Khaing, A., and Tipper, E. T.: Integrating Suspended Sediment Flux in Large Alluvial River Channels:
617 Application of a Synoptic Rouse-Based Model to the Irrawaddy and Salween Rivers, *Journal of Geophysical Research:*
618 *Earth Surface*, 125, <https://doi.org/10.1029/2020jfr005554>, 2020.
- 619 Bianchi, T. S.: The role of terrestrially derived organic carbon in the coastal ocean: A changing paradigm and the
620 priming effect, *Proceedings of the National Academy of Sciences*, 108, 19473–19481,
621 <https://doi.org/10.1073/pnas.1017982108>, 2011.
- 622 Bird, A., Stevens, T., Rittner, M., Vermeesch, P., Carter, A., Andò, S., Garzanti, E., Lu, H., Nie, J., Zeng, L., Zhang,
623 H., and Xu, Z.: Quaternary dust source variation across the Chinese Loess Plateau, *Palaeogeography,*
624 *Palaeoclimatology, Palaeoecology*, 435, 254–264, <https://doi.org/10.1016/j.palaeo.2015.06.024>, 2015.
- 625 Blair, N. E. and Aller, R. C.: The Fate of Terrestrial Organic Carbon in the Marine Environment, *Annual Review of*
626 *Marine Science*, 4, 401–423, <https://doi.org/10.1146/annurev-marine-120709-142717>, 2012.
- 627 Blair, N. E., Leithold, E. L., Brackley, H., Trustrum, N., Page, M., and Childress, L.: Terrestrial sources and export of
628 particulate organic carbon in the Waipaoa sedimentary system: Problems, progress and processes, *Marine Geology*,
629 270, 108–118, <https://doi.org/10.1016/j.margeo.2009.10.016>, 2010.
- 630 Bouchez, J., Galy, V., Hilton, R. G., Gaillardet, J., Moreira-Turcq, P., Pérez, M. A., France-Lanord, C., and Maurice,
631 L.: Source, transport and fluxes of Amazon River particulate organic carbon: Insights from river sediment depth-
632 profiles, *Geochimica et Cosmochimica Acta*, 133, 280–298, <https://doi.org/10.1016/j.gca.2014.02.032>, 2014.
- 633 Bouchez, J., Gaillardet, J., France-Lanord, C., Maurice, L., and Dutra-Maia, P.: Grain size control of river suspended
634 sediment geochemistry: Clues from Amazon River depth profiles, *Geochemistry, Geophysics, Geosystems*, 12, n/a-
635 n/a, <https://doi.org/10.1029/2010gc003380>, 2011a.
- 636 Bouchez, J., Lupker, M., Gaillardet, J., France-Lanord, C., and Maurice, L.: How important is it to integrate riverine
637 suspended sediment composition with depth? Clues from Amazon River depth-profiles, *Geochimica et*
638 *Cosmochimica Acta*, 75, 6955–6970, <https://doi.org/10.1016/j.gca.2011.08.038>, 2011.
- 639 Carignan, J., Hild, P., Mevelle, G., Morel, J., and Yeghicheyan, D.: Routine Analyses of Trace Elements in Geological
640 Samples using Flow Injection and Low Pressure On-Line Liquid Chromatography Coupled to ICP-MS: A Study of
641 Geochemical Reference Materials BR, DR-N, UB-N, AN-G and GH, *Geostandards Newsletter*, 25, 187–198,
642 <https://doi.org/10.1111/j.1751-908X.2001.tb00595.x>, 2001.



- 643 Cauwet, G. and Mackenzie, F. T.: Carbon inputs and distribution in estuaries of turbid rivers: the Yang Tze and Yellow
644 rivers (China), *Marine Chemistry*, 43, 235–246, [https://doi.org/10.1016/0304-4203\(93\)90229-h](https://doi.org/10.1016/0304-4203(93)90229-h), 1993.
- 645 Cheng, P., Burr, G. S., Zhou, W., Chen, N., Hou, Y., Du, H., Fu, Y., and Lu, X.: The deficiency of organic matter 14C
646 dating in Chinese Loess-paleosol sample, *Quaternary Geochronology*, 56, 101051,
647 <https://doi.org/10.1016/j.quageo.2019.101051>, 2020.
- 648 Curry, K. J., Bennett, R. H., Mayer, L. M., Curry, A., Abril, M., Biesiot, P. M., and Hulbert, M. H.: Direct visualization
649 of clay microfabric signatures driving organic matter preservation in fine-grained sediment, *Geochimica et*
650 *Cosmochimica Acta*, 71, 1709–1720, <https://doi.org/10.1016/j.gca.2007.01.009>, 2007.
- 651 Dellinger, M., Gaillardet, J., Bouchez, J., Calmels, D., Galy, V., Hilton, R. G., Louvat, P., and France-Lanord, C.:
652 Lithium isotopes in large rivers reveal the cannibalistic nature of modern continental weathering and erosion, *Earth*
653 *and Planetary Science Letters*, 401, 359–372, <https://doi.org/10.1016/j.epsl.2014.05.061>, 2014.
- 654 Freymond, C. V., Lupker, M., Peterse, F., Haghipour, N., Wacker, L., Filip, F., Giosan, L., and Eglinton, T. I.:
655 Constraining Instantaneous Fluxes and Integrated Compositions of Fluvially Discharged Organic Matter, *Geochem*
656 *Geophys Geosy*, 19, 2453–2462, <https://doi.org/10.1029/2018gc007539>, 2018.
- 657 Gaillardet, J., Dupré, B., Louvat, P., and Allègre, C. J.: Global silicate weathering and CO₂ consumption rates deduced
658 from the chemistry of large rivers, *Chemical Geology*, 159, 3–30, [https://doi.org/10.1016/s0009-2541\(99\)00031-5](https://doi.org/10.1016/s0009-2541(99)00031-5),
659 1999.
- 660 Galy, V. and Eglinton, T.: Protracted storage of biospheric carbon in the Ganges–Brahmaputra basin, *Nature Geosci*,
661 4, 843–847, <https://doi.org/10.1038/ngeo1293>, 2011.
- 662 Galy, V., Beyssac, O., France-Lanord, C., and Eglinton, T.: Recycling of graphite during Himalayan erosion: a
663 geological stabilization of carbon in the crust, *Science*, 322, 943–5, <https://doi.org/10.1126/science.1161408>, 2008a.
- 664 Galy, V., France-Lanord, C., and Lartiges, B.: Loading and fate of particulate organic carbon from the Himalaya to
665 the Ganga–Brahmaputra delta, *Geochimica et Cosmochimica Acta*, 72, 1767–1787,
666 <https://doi.org/10.1016/j.gca.2008.01.027>, 2008b.
- 667 Galy, V., France-Lanord, C., Beyssac, O., Faure, P., Kudrass, H., and Palhol, F.: Efficient organic carbon burial in the
668 Bengal fan sustained by the Himalayan erosional system, *Nature*, 450, 407–10, <https://doi.org/10.1038/nature06273>,
669 2007.
- 670 Galy, V., Peucker-Ehrenbrink, B., and Eglinton, T.: Global carbon export from the terrestrial biosphere controlled by
671 erosion, *Nature*, 521, 204–7, <https://doi.org/10.1038/nature14400>, 2015.
- 672 Garzanti, E., Andò, S., France-Lanord, C., Vezzoli, G., Censi, P., Galy, V., and Najman, Y.: Mineralogical and
673 chemical variability of fluvial sediments: 1. Bedload sand (Ganga–Brahmaputra, Bangladesh), *Earth and Planetary*
674 *Science Letters*, 299, 368–381, <https://doi.org/10.1016/j.epsl.2010.09.017>, 2010.
- 675 Garcia, M.: Sedimentation Engineering, *American Society of Civil Engineers*, (pp. 21-163)
676 <https://doi.org/10.1061/9780784408148>, 2008.
- 677 Ge, T., Xue, Y., Jiang, X., Zou, L., and Wang, X.: Sources and radiocarbon ages of organic carbon in different grain
678 size fractions of Yellow River-transported particles and coastal sediments, *Chemical Geology*, 534, 119452,
679 <https://doi.org/10.1016/j.chemgeo.2019.119452>, 2020.
- 680 Gu, Z., Duan, X., Shi, Y., Li, Y., and Pan, X.: Spatiotemporal variation in vegetation coverage and its response to
681 climatic factors in the Red River Basin, China, *Ecological Indicators*, 93, 54–64,
682 <https://doi.org/10.1016/j.ecolind.2018.04.033>, 2018.
- 683 Guo, H., Jia, W., Peng, P., Lei, Y., Luo, X., Cheng, M., Wang, X., Zhang, L., and Jiang, C.: The composition and its
684 impact on the methane sorption of lacustrine shales from the Upper Triassic Yanchang Formation, Ordos Basin, China,
685 *Marine and Petroleum Geology*, 57, 509–520, <https://doi.org/10.1016/j.marpetgeo.2014.05.010>, 2014.
- 686 Guo, K., Zou, T., Jiang, D., Tang, C., and Zhang, H.: Variability of Yellow River turbid plume detected with satellite
687 remote sensing during water-sediment regulation, *Continental Shelf Research*, 135, 74–85,
688 <https://doi.org/10.1016/j.csr.2017.01.017>, 2017.
- 689 Guo, L., Ping, C.-L., and Macdonald, R. W.: Mobilization pathways of organic carbon from permafrost to arctic rivers
690 in a changing climate, *Geophysical Research Letters*, 34, <https://doi.org/10.1029/2007GL030689>, 2007.
- 691 Guo, Z. T., Ruddiman, W. F., Hao, Q. Z., Wu, H. B., Qiao, Y. S., Zhu, R. X., Peng, S. Z., Wei, J. J., Yuan, B. Y., and
692 Liu, T. S.: Onset of Asian desertification by 22 Myr ago inferred from loess deposits in China, *Nature*, 416, 159–163,
693 <https://doi.org/10.1038/416159a>, 2002.
- 694 Hatte, C., Tisnerat-Laborde, N., Ayrault, S., Balesdent, J., Chapon, V., Bourguignon, J., Alban, C., Ravanel, S.,
695 Denaix, L., Nguyen, C., Vavasseur, A., Sarrobert, C., Gasperi, J., Latrille, C., Savoye, S., Augusto, L., Conan Labbe,
696 A., Bernard Michel, B., Douysset, G., Toqnelli, A., Vailhen, D., and Moulin, C.: Soil, climate and the environment -
697 an indissociable threesome Soil carbon and global changes: reciprocal impacts; Carbon in all its forms; Echomicadas,
698 a new tool to analyse carbon 14; Biotransformation of metallic trace elements by soil micro-organisms; Absorption



- 699 and distribution of metallic elements in plants; Dynamics of metallic contaminants in agricultural systems; Is photo-
700 remediation for tomorrow? Hyper-accumulator plants; Sediments, tell me the Seine history The complex history of
701 plant feeding by the soil; The environmental analysis, Biofutur (Paris), 26–57, 2016.
- 702 He, X., Zhou, J., Zhang, X., and Tang, K.: Soil erosion response to climatic change and human activity during the
703 Quaternary on the Loess Plateau, China, *Reg Environ Change*, 6, 62–70, <https://doi.org/10.1007/s10113-005-0004-7>,
704 2006.
- 705 Hemingway, J. D., Hilton, R. G., Hovius, N., Eglinton, T. I., Haghypour, N., Wacker, L., Chen, M. C., and Galy, V.
706 V.: Microbial oxidation of lithospheric organic carbon in rapidly eroding tropical mountain soils, *Science*, 360, 209–
707 212, <https://doi.org/10.1126/science.aao6463>, 2018.
- 708 Hemingway, J. D., Rothman, D. H., Grant, K. E., Rosengard, S. Z., Eglinton, T. I., Derry, L. A., and Galy, V. V.:
709 Mineral protection regulates long-term global preservation of natural organic carbon, *Nature*, 570, 228–231,
710 <https://doi.org/10.1038/s41586-019-1280-6>, 2019.
- 711 Hilton, R. G., Gaillardet, J., Calmels, D., and Birck, J.-L.: Geological respiration of a mountain belt revealed by the
712 trace element rhenium, *Earth and Planetary Science Letters*, 403, 27–36, <https://doi.org/10.1016/j.epsl.2014.06.021>,
713 2014.
- 714 Hilton, R. G., Galy, A., Hovius, N., Hornig, M.-J., and Chen, H.: Efficient transport of fossil organic carbon to the
715 ocean by steep mountain rivers: An orogenic carbon sequestration mechanism, *Geology*, 39, 71–74,
716 <https://doi.org/10.1130/g31352.1>, 2011.
- 717 Hilton, R. G., Galy, V., Gaillardet, J., Dellinger, M., Bryant, C., O'Regan, M., Grocke, D. R., Coxall, H., Bouchez, J.,
718 and Calmels, D.: Erosion of organic carbon in the Arctic as a geological carbon dioxide sink, *Nature*, 524, 84–7,
719 <https://doi.org/10.1038/nature14653>, 2015.
- 720 Hu, B., Li, J., Bi, N., Wang, H., Wei, H., Zhao, J., Xie, L., Zou, L., Cui, R., Li, S., Liu, M., and Li, G.: Effect of
721 human-controlled hydrological regime on the source, transport, and flux of particulate organic carbon from the lower
722 Huanghe (Yellow River), *Earth Surface Processes and Landforms*, 40, 1029–1042, <https://doi.org/10.1002/esp.3702>,
723 2015.
- 724 Hua, Q., Barbetti, M., and Rakowski, A. Z.: Atmospheric Radiocarbon for the Period 1950–2010, *Radiocarbon*, 55,
725 2059–2072, https://doi.org/10.2458/azu_js_rc.v55i2.16177, 2013.
- 726 Huang, C. C., and Ren, Z.: Fluvial erosion and the formation of gully systems over the Chinese Loess Plateau, *WSEAS*
727 *Transactions on Environment and Development*, 2(2), 141–145, 2006.
- 728 Jahn, B., Gallet, S., and Han, J.: Geochemistry of the Xining, Xifeng and Jixian sections, Loess Plateau of China:
729 eolian dust provenance and paleosol evolution during the last 140 ka, *Chemical Geology*, 178, 71–94,
730 [https://doi.org/10.1016/S0009-2541\(00\)00430-7](https://doi.org/10.1016/S0009-2541(00)00430-7), 2001.
- 731 Ke, Y., Calmels, D., Bouchez, J., and Quantin, C.: MODern River archivES of Particulate Organic Carbon:
732 MOREPOC, *Earth System Science Data Discussions*, 1–19, <https://doi.org/10.5194/essd-2022-161>, 2022.
- 733 Keil, R. G., Mayer, L. M., Quay, P. D., Richey, J. E., and Hedges, J. I.: Loss of organic matter from riverine particles
734 in deltas, *Geochimica et Cosmochimica Acta*, 61, 1507–1511, [https://doi.org/10.1016/S0016-7037\(97\)00044-6](https://doi.org/10.1016/S0016-7037(97)00044-6), 1997.
- 735 Gen Li, X. T. W., Zhongfang Yang, Changping Mao, A. Joshua West, Junfeng Ji: Dam-triggered organic carbon
736 sequestration makes the Changjiang (Yangtze) river basin (China) a significant carbon sink, *Journal of Geophysical*
737 *Research: Biogeosciences*, 2015.
- 738 Licht, A., Pullen, A., Kapp, P., Abell, J., and Giesler, N.: Eolian cannibalism: Reworked loess and fluvial sediment as
739 the main sources of the Chinese Loess Plateau, *GSA Bulletin*, 128, 944–956, <https://doi.org/10.1130/B31375.1>, 2016.
- 740 Liu, G., Xu, W., Zhang, Q., & Xia, Z.: Holocene Soil Chronofunctions, Luochuan, Chinese Loess Plateau.
741 *Radiometric Dating*, 41, 2012.
- 742 Liu, J. and Liu, W.: Soil nitrogen isotopic composition of the Xifeng loess-paleosol sequence and its potential for use
743 as a paleoenvironmental proxy, *Quaternary International*, 440, 35–41, <https://doi.org/10.1016/j.quaint.2016.04.018>,
744 2017.
- 745 Liu, W., Yang, H., Ning, Y., and An, Z.: Contribution of inherent organic carbon to the bulk $\delta^{13}\text{C}$ signal in loess
746 deposits from the arid western Chinese Loess Plateau, *Organic Geochemistry*, 38, 1571–1579,
747 <https://doi.org/10.1016/j.orggeochem.2007.05.004>, 2007.
- 748 Ludwig, W., Probst, J.-L., and Kempe, S.: Predicting the oceanic input of organic carbon by continental erosion,
749 *Global Biogeochemical Cycles*, 10, 23–41, <https://doi.org/10.1029/95gb02925>, 1996.
- 750 Mayorga, E., Aufdenkampe, A. K., Masiello, C. A., Krusche, A. V., Hedges, J. I., Quay, P. D., Richey, J. E., and
751 Brown, T. A.: Young organic matter as a source of carbon dioxide outgassing from Amazonian rivers, *Nature*, 436,
752 538–41, <https://doi.org/10.1038/nature03880>, 2005.
- 753 Milliman, J. D. and Farnsworth, K. L.: River discharge to the coastal ocean: a global synthesis, Cambridge University
754 Press, 2011.



- 755 Milliman, J. D., Yun-Shan, Q., Mei-E, R., and Saito, Y.: Man's Influence on the Erosion and Transport of Sediment
756 by Asian Rivers: The Yellow River (Huanghe) Example, *The Journal of Geology*, 95, 751–762,
757 <https://doi.org/10.1086/629175>, 1987.
- 758 Moodie, A. J., Nittrouer, J. A., Ma, H., Carlson, B. N., Wang, Y., Lamb, M. P., and Parker, G.: Suspended Sediment-
759 Induced Stratification Inferred From Concentration and Velocity Profile Measurements in the Lower Yellow River,
760 China, *Water Resources Research*, 58, e2020WR027192, <https://doi.org/10.1029/2020WR027192>, 2022.
- 761 Ning, Y., Liu, W., and An, Z.: Variation of soil $\delta^{13}\text{C}$ values in Xifeng loess-paleosol sequence and its
762 paleoenvironmental implication, *CHINESE SCI BULL.*, 51, 1350–1354, <https://doi.org/10.1007/s11434-006-1350-7>,
763 2006.
- 764 Pan, B., Pang, H., Gao, H., Garzanti, E., Zou, Y., Liu, X., Li, F., and Jia, Y.: Heavy-mineral analysis and provenance
765 of Yellow River sediments around the China Loess Plateau, *Journal of Asian Earth Sciences*, 127, 1–11,
766 <https://doi.org/10.1016/j.jseaeas.2016.06.006>, 2016.
- 767 Qu, Y., Jin, Z., Wang, J., Wang, Y., Xiao, J., Gou, L.-F., Zhang, F., Liu, C.-Y., Gao, Y., Suarez, M. B., and Xu, X.:
768 The sources and seasonal fluxes of particulate organic carbon in the Yellow River, *Earth Surface Processes and
769 Landforms*, <https://doi.org/10.1002/esp.4861>, 2020.
- 770 Ran, L., Lu, X. X., and Xin, Z.: Erosion-induced massive organic carbon burial and carbon emission in the Yellow
771 River basin, China, *Biogeosciences*, 11, 945–959, <https://doi.org/10.5194/bg-11-945-2014>, 2014.
- 772 Ran, L., Lu, X. X., Sun, H., Han, J., Li, R., and Zhang, J.: Spatial and seasonal variability of organic carbon transport
773 in the Yellow River, China, *Journal of Hydrology*, 498, 76–88, <https://doi.org/10.1016/j.jhydrol.2013.06.018>, 2013.
- 774 Rao, Z., Guo, W., Cao, J., Shi, F., Jiang, H., and Li, C.: Relationship between the stable carbon isotopic composition
775 of modern plants and surface soils and climate: A global review, *Earth-Science Reviews*, 165, 110–119,
776 <https://doi.org/10.1016/j.earscirev.2016.12.007>, 2017.
- 777 Rouse, H.: Modern Conceptions of the Mechanics of Fluid Turbulence, *Transactions of the American Society of Civil
778 Engineers*, 102, 463–505, <https://doi.org/10.1061/TACEAT.0004872>, 1937.
- 779 Shi, H. and Shao, M.: Soil and water loss from the Loess Plateau in China, *Journal of Arid Environments*, 45, 9–20,
780 <https://doi.org/10.1006/jare.1999.0618>, 2000.
- 781 Stevens, T., Carter, A., Watson, T. P., Vermeesch, P., Andò, S., Bird, A. F., Lu, H., Garzanti, E., Cottam, M. A., and
782 Sevastjanova, I.: Genetic linkage between the Yellow River, the Mu Us desert and the Chinese Loess Plateau,
783 *Quaternary Science Reviews*, 78, 355–368, <https://doi.org/10.1016/j.quascirev.2012.11.032>, 2013.
- 784 Sun, D., Tang, J., He, Y., Liao, W., and Sun, Y.: Sources, distributions, and burial efficiency of terrigenous organic
785 matter in surface sediments from the Yellow River mouth, northeast China, *Organic Geochemistry*, 118, 89–102,
786 <https://doi.org/10.1016/j.orggeochem.2017.12.009>, 2018.
- 787 Syvitski, J. P. M., Vörösmarty, C. J., Kettner, A. J., and Green, P.: Impact of Humans on the Flux of Terrestrial
788 Sediment to the Global Coastal Ocean, *Science*, 308, 376–380, <https://doi.org/10.1126/science.1109454>, 2005.
- 789 Tao, S., Eglinton, T. I., Montluçon, D. B., McIntyre, C., and Zhao, M.: Pre-aged soil organic carbon as a major
790 component of the Yellow River suspended load: Regional significance and global relevance, *Earth and Planetary
791 Science Letters*, 414, 77–86, <https://doi.org/10.1016/j.epsl.2015.01.004>, 2015.
- 792 Tao, S., Eglinton, T. I., Montluçon, D. B., McIntyre, C., and Zhao, M.: Diverse origins and pre-depositional histories
793 of organic matter in contemporary Chinese marginal sea sediments, *Geochimica et Cosmochimica Acta*, 191, 70–88,
794 <https://doi.org/10.1016/j.gca.2016.07.019>, 2016.
- 795 Tao, S., Eglinton, T. I., Zhang, L., Yi, Z., Montluçon, D. B., McIntyre, C., Yu, M., and Zhao, M.: Temporal variability
796 in composition and fluxes of Yellow River particulate organic matter, *Limnology and Oceanography*, 63, S119–S141,
797 <https://doi.org/10.1002/lno.10727>, 2018.
- 798 Walling, D. E. and Fang, D.: Recent trends in the suspended sediment loads of the world's rivers, *Global and Planetary
799 Change*, 39, 111–126, [https://doi.org/10.1016/S0921-8181\(03\)00020-1](https://doi.org/10.1016/S0921-8181(03)00020-1), 2003.
- 800 Wang, C., Li, F., Shi, H., Jin, Z., Sun, X., Zhang, F., Wu, F., and Kan, S.: The significant role of inorganic matters in
801 preservation and stability of soil organic carbon in the Baoji and Luochuan loess/paleosol profiles, Central China,
802 *CATENA*, 109, 186–194, <https://doi.org/10.1016/j.catena.2013.04.001>, 2013.
- 803 Wang, G., Feng, X., Han, J., Zhou, L., Tan, W., and Su, F.: Paleovegetation reconstruction using $\delta^{13}\text{C}$ of Soil Organic
804 Matter, *Biogeosciences*, 5, 1325–1337, <https://doi.org/10.5194/bg-5-1325-2008>, 2008.
- 805 Wang, H., Bi, N., Saito, Y., Wang, Y., Sun, X., Zhang, J., and Yang, Z.: Recent changes in sediment delivery by the
806 Huanghe (Yellow River) to the sea: Causes and environmental implications in its estuary, *Journal of Hydrology*, 391,
807 302–313, <https://doi.org/10.1016/j.jhydrol.2010.07.030>, 2010.
- 808 Wang, H., Wu, X., Bi, N., Li, S., Yuan, P., Wang, A., Syvitski, J. P. M., Saito, Y., Yang, Z., Liu, S., and Nittrouer, J.:
809 Impacts of the dam-orientated water-sediment regulation scheme on the lower reaches and delta of the Yellow River



- 810 (Huanghe): A review, *Global and Planetary Change*, 157, 93–113, <https://doi.org/10.1016/j.gloplacha.2017.08.005>,
811 2017.
- 812 Wang, H., Yang, Z., Saito, Y., Liu, J. P., Sun, X., and Wang, Y.: Stepwise decreases of the Huanghe (Yellow River)
813 sediment load (1950–2005): Impacts of climate change and human activities, *Global and Planetary Change*, 57, 331–
814 354, <https://doi.org/10.1016/j.gloplacha.2007.01.003>, 2007.
- 815 Wang, S., Fu, B., Piao, S., Lü, Y., Ciais, P., Feng, X., and Wang, Y.: Reduced sediment transport in the Yellow River
816 due to anthropogenic changes, *Nature Geosci*, 9, 38–41, <https://doi.org/10.1038/ngeo2602>, 2016.
- 817 Wang, X., Xu, C., Druffel, E. M., Xue, Y., and Qi, Y.: Two black carbon pools transported by the Changjiang and
818 Huanghe Rivers in China, *Global Biogeochemical Cycles*, 2016.
- 819 Weiguo, L., Xiahong, F., Youfeng, N., Qingle, Z., Yunning, C., and Zhisheng, A. N.: $\delta^{13}\text{C}$ variation of C3 and C4
820 plants across an Asian monsoon rainfall gradient in arid northwestern China, *Global Change Biology*, 11, 1094–1100,
821 <https://doi.org/10.1111/j.1365-2486.2005.00969.x>, 2005.
- 822 Xiubin, H., Tang, K., and Zhang, X.: Soil Erosion Dynamics on the Chinese Loess Plateau in the Last 10,000 Years,
823 *mred*, 24, 342–347, [https://doi.org/10.1659/0276-4741\(2004\)024\[0342:SEDOTC\]2.0.CO;2](https://doi.org/10.1659/0276-4741(2004)024[0342:SEDOTC]2.0.CO;2), 2004.
- 824 Yu, M., Eglinton, T. I., Haghypour, N., Montluçon, D. B., Wacker, L., Hou, P., Zhang, H., and Zhao, M.: Impacts of
825 Natural and Human-Induced Hydrological Variability on Particulate Organic Carbon Dynamics in the Yellow River,
826 *Environ Sci Technol*, 53, 1119–1129, <https://doi.org/10.1021/acs.est.8b04705>, 2019a.
- 827 Yu, M., Eglinton, T. I., Haghypour, N., Montluçon, D. B., Wacker, L., Wang, Z., Jin, G., and Zhao, M.: Molecular
828 isotopic insights into hydrodynamic controls on fluvial suspended particulate organic matter transport, *Geochimica et*
829 *Cosmochimica Acta*, 262, 78–91, <https://doi.org/10.1016/j.gca.2019.07.040>, 2019b.
- 830 Zhang, L. J., Wang, L., Cai, W. J., Liu, D. M., and Yu, Z. G.: Impact of human activities on organic carbon transport
831 in the Yellow River, *Biogeosciences*, 10, 2513–2524, <https://doi.org/10.5194/bg-10-2513-2013>, 2013.
- 832 Zhu, T. X.: Gully and tunnel erosion in the hilly Loess Plateau region, China, *Geomorphology*, 153–154, 144–155,
833 <https://doi.org/10.1016/j.geomorph.2012.02.019>, 2012.